TREATMENT REQUIREMENTS FOR IRRADIATED RBMK-1500 GRAPHITE TO MEET DISPOSAL REQUIREMENTS IN LITHUANIA

P. POSKAS, E. NARKUNAS, A. SMAIZYS

Nuclear Engineering Laboratory
Lithuanian Energy Institute
Lithuania

Abstract

The work presented in this report was focused on the modelling of the induced activity spatial distribution in the RBMK-1500 reactor graphite components. The performed modelling may be divided into two separate stages – modelling of neutron fluxes in the reactor graphite components and modelling of radionuclides activation in the mentioned components using already modelled neutron fluxes. In such way, the spatial induced activity distribution in the analysed reactor components was obtained. For this CRP, the modelling of radial neutron fluxes distribution in the reactor RBMK-1500 graphite blocks and rings/sleeves was performed and distribution of neutron flux was evaluated. Then, using averaged neutron fluxes in the lateral direction of the graphite components, neutron activation modelling was performed and the axial induced activity distribution in the graphite blocks and rings/sleeves was obtained for both (Unit 1 & 2) Ignalina NPP RBMK-1500 reactors, taking into account their individual operation histories. Furthermore, the influence of different data libraries and different fuel compositions for neutron fluxes modelling was analysed as well as the influence of different initial impurities concentrations in the graphite for activation modelling. Then the analysis of spatial distribution of selected radionuclides in graphite blocks and rings/sleeves was made for Ignalina NPP Unit 2 RBMK-1500 reactor components. For this, each of the reactor graphite components was divided into three segments (inner, middle and outer) and neutron fluxes in these segments were evaluated. Then, using these neutron fluxes in each of the segment and only Unit 2 operation history, neutron activation modelling was performed and the spatial (axial + radial) induced activity distribution in the graphite blocks and rings/sleeves was obtained. Results are presented for radionuclides H-3, C-14 and Cl-36 that are usually of the most concern in the irradiated graphite.

1. INTRODUCTION

There are two RBMK-1500 water-cooled graphite-moderated channel-type power reactors at Ignalina Nuclear Power Plant (Ignalina NPP) in Lithuania. Both reactors are under decommissioning now. The graphite stack of each reactor consist of 2488 individual 8 m height graphite columns and serves as a neutron moderator and reflector. Each column consists of several graphite blocks made of GR-280 grade graphite, which are stacked on each other. Technological channels are placed within the graphite columns. In order to improve the heat transfer from the graphite columns, split rings and sleeves made of GRP-2-125 grade graphite are surrounding the parts of the technological channels within the stack. The mass of these graphite components in one reactor is about 1900 tonnes.

Currently, in general, the geological disposal of irradiated graphite is accepted worldwide, as without treatment it usually does not meet the waste acceptance criteria for near surface disposal. Partial removal of particular radionuclide(s) from graphite (i.e. partial decontamination of graphite) or its immobilisation are of great importance because this could enable disposal of appropriately treated graphite into the near surface repositories. This means that the knowledge of radiological inventory and the spatial distribution of particular radionuclide(s) in different reactor graphite component is very important, because it may determine/indicate selection of appropriate treatment method(s) for the irradiated graphite in order to remove specific radionuclide(s) or immobilise it.

Based on that, this work concentrated on the modelling of radionuclides inventories and their distributions in the irradiated RBMK-1500 reactor graphite components. This report presents the

results of the modelling of neutron flux distributions in the reactor RBMK-1500 graphite blocks and rings/sleeves and the results of induced activity distribution in these components. Neutron activation modelling was performed for both Ignalina NPP RBMK-1500 reactors, taking into account their individual operation histories. The influence of different data libraries, different fuel compositions and different initial impurities concentrations is also analysed and presented.

2. METHODOLOGY

The assessment of the neutron induced activities requires, as a first step, knowledge of the spatial and energy distributions of the neutron fluxes throughout the system. The neutron fluxes are then used for calculation of the specific component activity from the known concentration of the initial chemical elements in the material, from which the component is manufactured. A general methodology involved in the inventory calculation of neutron activated materials is summarized in FIG. 1 [1].

FIG. 1. General methodology for neutron induced activity calculations [1].

The neutron flux modelling and subsequent inventory calculations (activation modelling) were performed using MCNP 6 and ORIGEN-S (SCALE 5) computer codes.

The cross-section of INPP RBMK-1500 reactor vault is presented in FIG. 2 [2]. The model developed in this work for the neutron flux modelling and subsequent neutron activation analysis of graphite components is marked as item 12 in FIG. 2.

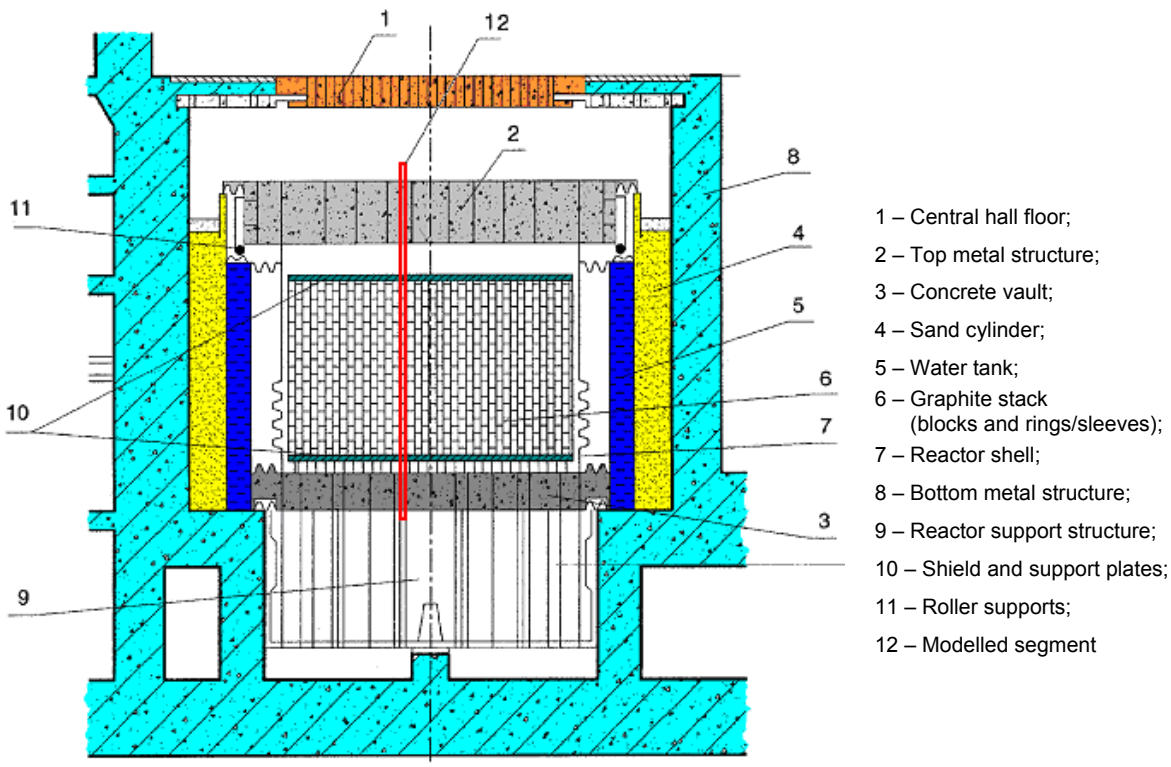

FIG. 2. Cross-section of RBMK-1500 reactor vault [2].

2.1. Initial materials compositions

Neutron activation and spatial distribution of induced activities was estimated for the graphite blocks (GR-280 grade graphite) and graphite rings/sleeves (GRP-2-125 grade graphite) of RBMK-1500 reactor, as indicated in TABLE 1.

TABLE 1. CONSTRUCTION MATERIALS OF THE RBMK-1500 REACTOR GRAPHITE COMPONENTS

Reactor Component	Structural Element	Material of Construction	Mass (tones)
Graphite stack	Graphite blocks	Graphite GR-280	~1800
	Graphite rings/sleeves	Graphite GRP-2-125	~100

Chemical compositions and concentrations of the elements (main elements and impurities) of these reactor graphite components were defined based on the data presented in the available scientific and technical literature for the specific material. It was assumed that the isotopic composition of each chemical element is the same as the naturally occurring isotopic content. Due to the lack of representative information on the materials compositions of the graphite components of Ignalina NPP reactors, materials' composition with maximal concentrations of impurities were assumed for the neutron activation assessment for both reactors in this work. However, for the assessment of impact of impurities concentrations on the modelled specific activity results, minimal impurities concentrations for Unit 2 graphite components were used also. Maximal and minimal impurities concentrations in GR-280 and GRP-2-125 grade graphite were gathered from the available published sources.

2.2. Modelling of spatial and energetic distribution of neutron fluxes

The spatial and energy distributions of the neutron flux within analysed reactor RBMK-1500 graphite components were evaluated via numerical modelling. MCNP 6 computer code was chosen for neutron

flux modelling, as this code successfully solves neutron transport problems almost in any 3D geometries and materials configurations.

Various data of the RBMK-1500 reactor were used while developing MCNP 6 model. These data are: geometrics of the reactor components, materials compositions and densities, reactor operation parameters and others. These data were based on the information presented in [2], [3], [4]. In order to assess the impact of different fuel types (fuel with and without burnable erbium absorber) and different fuel burnups on the neutron flux distributions, 3 cases of one lattice segment model were developed firstly, assuming that:

1. Fuel channel is loaded with UO_2 fuel of average burnup of ~10 MWd/kgU with 2.4 % U-235 enrichment and 0.41 % burnable Er_2O_3 absorber content;

2. Fuel channel is loaded with fresh UO_2 fuel with 2.4 % U-235 enrichment and 0.41 % burnable Er_2O_3 absorber content;

3. Fuel channel is loaded with fresh UO_2 fuel with 2.0 % U-235 enrichment.

Taking into the consideration the information on the usage of nuclear fuel with different enrichments and absorber contents and the information on the average fuel burnup within the reactor core, the neutron flux modelling results obtained using the first model case were selected to be used as a basis in the subsequent neutron activation modelling of the reactors graphite components. The radionuclides inventory of spent nuclear fuel (with burnup up to ~10 MWd/kgU) was modelled by computer code SAS2 from SCALE 5 computer code system. It was assumed that fuel assembly (FA), which consists of two fuel bundles with UO_2 fuel (2.4 % U-235 enrichment and 0.41 % burnable Er_2O_3 absorber) of ~10 MWd/kgU burnup is placed in a fuel channel (FC). The parameters of all described reactor components (temperatures, densities, dimensions, etc.) were set so that they correspond to the conditions of the fuel channel working on the average power (~2.61 MW), corresponding to the nominal 4200 MW reactor thermal power.

A view of cross-section of the first case one lattice segment model (25×25 cm) of the Ignalina NPP RBMK-1500 reactor (item 12 in FIG. 2), developed with MCNP 6 code, is presented in FIG. 3 a). It should be noted, that 2nd and 3rd model cases are exactly the same, except the fuel composition.

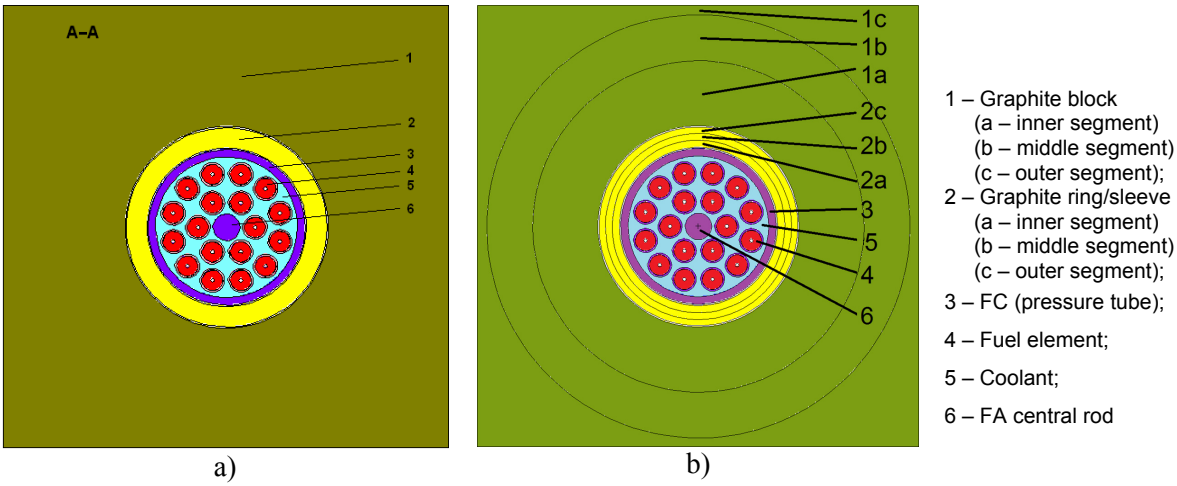

a) b)

FIG. 3. Cross-section of the modelled segment of the RBMK-1500 reactor (throughout fuel bundle).

The developed model itself, enveloping the graphite column with other elements inside it, shield and support plates, top and bottom metal structures with serpentinite fillings, etc., including geometrical data, is given in FIG. 4.

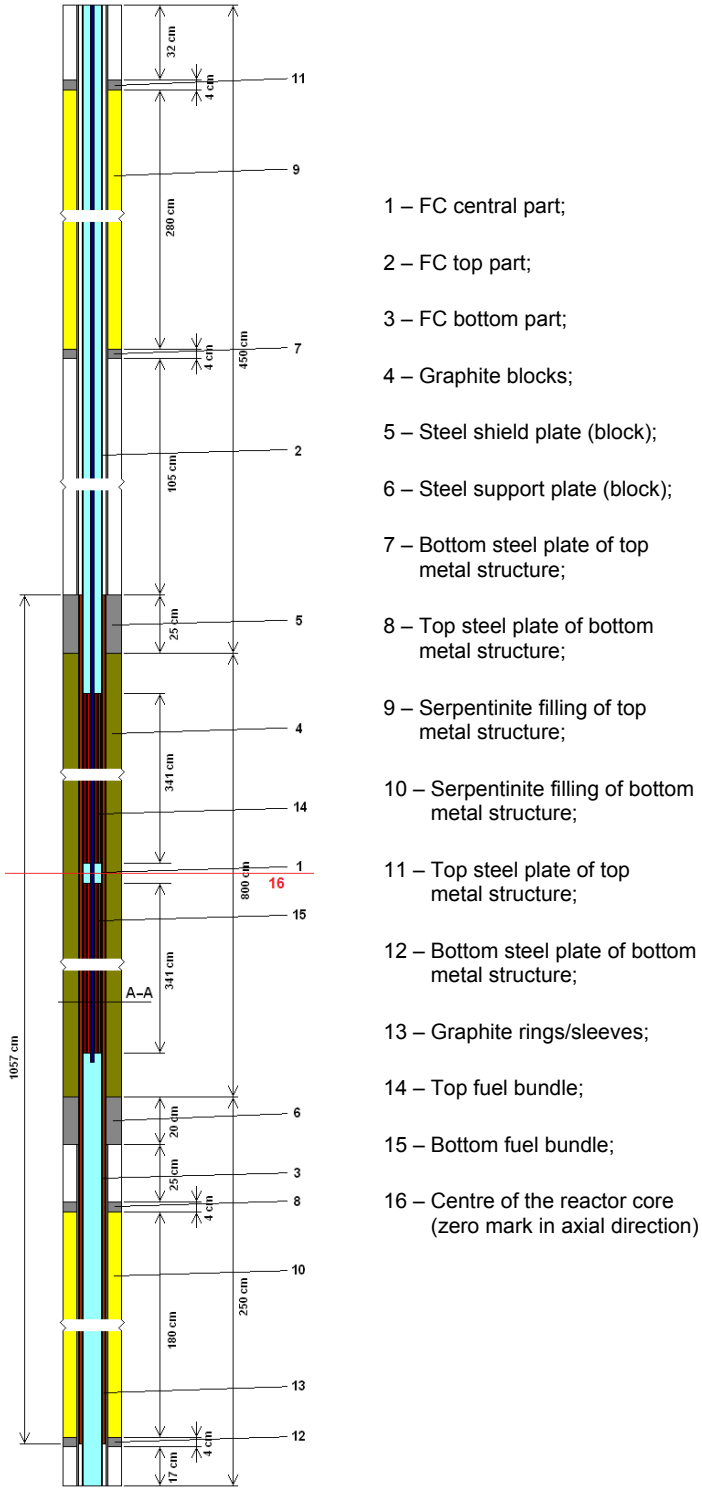

FIG. 4. The analysed segment of the RBMK-1500 reactor, developed with MCNP 6 code.

This model of one reactor lattice cell segment, using periodic boundary conditions for the side walls of the segment, corresponds to an infinite lattice comprised of such segments and is suitable for modelling of neutron fluxes in the reactor graphite elements of the central (in radial direction) core part (plateau). However, this approach is conservative because the impact of the surrounding FC with control rods in the vicinity of the analysed segment is not taken into account.

The first model case was also used for the evaluation of the different nuclear data libraries impact on the modelled neutron fluxes. Three data libraries (LLNL, ENDF/B-V and ENDF/B-VI), distributed with MCNP 6 code package, were selected for this purpose.

Neutron fluxes, obtained using above mentioned 3 cases of one lattice cell model (FIG. 3 a), FIG. 4), were averaged over the whole cross-section of each graphite component in the lateral (radial) direction and over the heights of 50 cm in the axial direction. This enabled the axial distribution of these laterally averaged fluxes in the particular graphite component to be obtained and these fluxes were used as a basis for the neutron activation modelling of the reactors graphite components for both Units.

In order to evaluate the radial distribution of neutron fluxes in the graphite blocks and rings/sleeves, the first case of one lattice cell model was modified dividing graphite blocks and rings/sleeves into the three segments in the radial direction – inner, middle and outer, as presented in FIG. 3 b). The inner segment of each component (block and ring/sleeve) represents the part which is closest to the fuel channel while the outer – the one that is furthest. The segmentation was made in the way that the areas (and thus volumes) of each segment were equal, i.e. cross-section areas of all three segments are the same for the particular component. The fluxes obtained were averaged over the cross-section of each segment of the graphite component in the lateral (radial) direction and over the heights of 50 cm in the axial direction. In this way spatial (axial and radial) neutron flux distributions were obtained. These fluxes then were used for the evaluation of spatial distribution of induced activities of particular radionuclides in the graphite blocks and rings/sleeves of Unit 2 reactor.

For all cases, the neutron fluxes estimated with MCNP 6, were grouped into the three energy groups:

- Thermal neutrons, with energies up to 0.625 eV;
- Resonance neutrons, with energies in range of 0.625 eV – 1 MeV;
- Fast neutrons, with energies above 1 MeV.

2.3. Modelling of neutron activation of graphite components

ORIGEN-S computer code (SCALE 5 codes system) was used for the neutron activation modelling. The code considers radioactive disintegration and neutron absorption (capture and fission) and enables quantification of isotopic content, activities and concentrations of neutron activated materials. The rate of the change with time of the concentration for a particular nuclide N_i can be written as (1):

$$\frac{dN_i}{dt} = \sum_j \gamma_{ji}\sigma_{f,j}N_j\phi + \sigma_{c,i-1}N_{i-1}\phi + \lambda_i^{'}N_i^{'} - \sigma_{f,i}N_i\phi - \sigma_{c,i}N_i\phi - \lambda_i N_i, \quad i = 1,\ldots I; \qquad (1)$$

where:

$\sum_j \gamma_{ji}\sigma_{f,j}N_j\phi$ – the yield rate of N_i due to the fission of all nuclides N_j;

$\sigma_{c,i-1}N_{i-1}\phi$ – the rate of transmutation into N_i, due to radiative neutron capture by a nuclide N_{i-1};

$\lambda_i^{'}N_i^{'}$ – the rate of formation of N_i due to the radioactive decay of nuclides $N_i^{'}$;

$\sigma_{f,i}N_i\phi$ – the destruction rate of N_i due to fission;

$\sigma_{c,i}N_i\phi$ – the destruction rate of N_i due to all forms of neutron absorption other than fission (n, γ), (n, α), (n, p), (n, 2n), (n, 3n);

$\lambda_i N_i$ – the radioactive decay rate of N_i.

The ORIGEN-S was used as a standalone program and the input data associated with neutron fluxes for neutron activation analysis were taken from the neutron flux modelling results.

The operation histories of Ignalina NPP Unit 1 and Unit 2 reactors were also taken into account for the neutron activation modelling, as presented in FIG. 5 and FIG. 6.

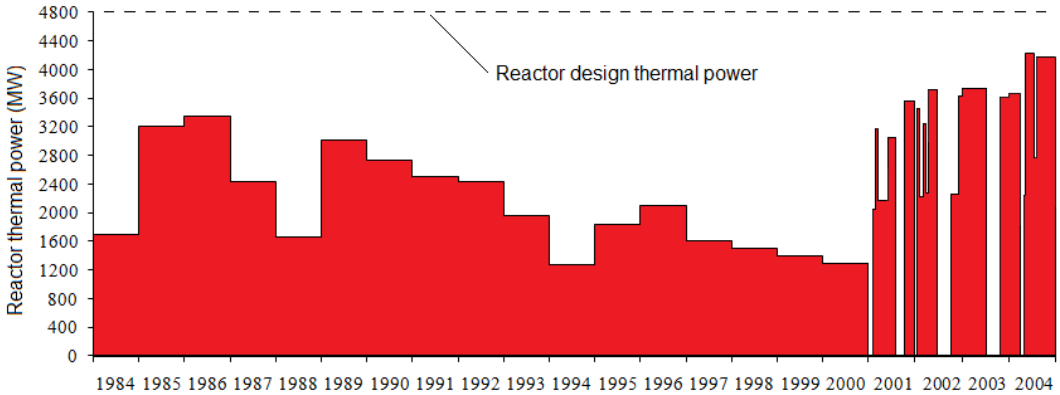

FIG. 5. The Ignalina NPP Unit 1 reactor operation history data for 1984–2004 year.

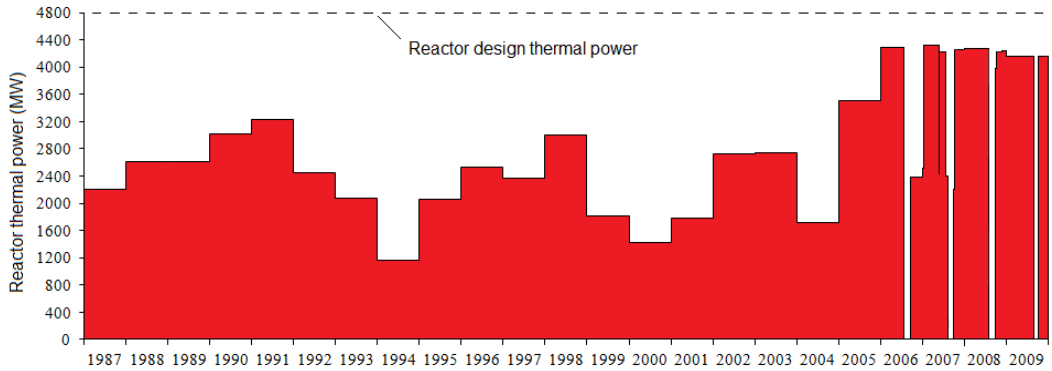

FIG. 6. The Ignalina NPP Unit 2 reactor operation history data for 1987–2009 year.

Separate modelling of the graphite components neutron activation for each Ignalina NPP reactor allows differences in of activated graphite inventories to be accommodated for different operational histories of the reactors.

As it was already mentioned, maximal impurities concentrations in the graphite components were used for all activation modelling cases here, except the assessment of impact of impurities concentrations, where minimal impurities concentrations were used also. Only the Ignalina NPP Unit 2 reactor operation history was used for this purpose.

The results of modelling of spatial (axial and radial) distributions of induced activities in the graphite blocks and rings/sleeves are presented for three radionuclides – H-3, C-14 and Cl-36. These radionuclides were selected because H-3 and C-14 could be the major radionuclides in the terms of activity in the irradiated graphite, first being short-lived while the second being long-lived. Cl-36 is not the main contributor to the activity of irradiated graphite, but being very long-lived and mobile in the disposal conditions, this radionuclide could be important for performance assessments of repositories.

A detailed comparison of these three radionuclide activities is also provided with the results, when analysing influence of the impurities concentrations for the induced activities.

3. RESULTS AND DISCUSSION

3.1. Spatial and energetic neutron flux distributions

Neutron fluxes were estimated in the graphite blocks and rings/sleeves of RBMK-1500 reactor. All modelled fluxes represent reactor operation at the nominal 4200 MW thermal power, i.e. at ~2.6 MW thermal power for one FC and are the same for both Ignalina NPP reactors. Furthermore, the modelled fluxes, presented here, are normalised to the maximal value of the neutron flux in the particular figure. Top 0.5 m thick and bottom 0.5 m thick layers of graphite stack in the axial direction are called top and bottom reflectors respectively, while remaining 7 m thick middle part – active zone. For convenience purpose, the axial distance from the centre of the reactor core is given in the ordinate axis in the respective figures of the subchapters 3.1 and 3.2, assuming that the centre of the core is at zero mark.

3.1.1. Spatial distributions of neutron fluxes

3.1.1.1. Radial (lateral) distributions

Radial distributions of the modelled thermal, resonance and fast neutron fluxes using one lattice cell first model (at different heights in the axial direction) are presented in FIG. 7. Neutron fluxes presented in FIG. 7 are given at five different characteristic heights of the modelled cell. They represent radial distribution of neutron fluxes in the middle plane of the top reflector, in the middle plane of the upper fuel bundle, in the middle plane between the top and the bottom fuel bundles, in the middle plane of the lower fuel bundle and in the middle plane of the bottom reflector. In this figure, the left column (or FIG. 7 a)) shows distributions of fast neutron fluxes, middle column (or FIG. 7 b)) – of resonance and right column (or FIG. 7 c)) – of thermal neutron fluxes.

Results clearly show, that for the heights corresponding to the centres of the upper and lower fuel bundles, thermal neutrons (FIG. 7 c)) are dominant in the graphite block (where moderation of the fast and resonance neutrons generally takes place). For the fuel channel (marked with the inner and middle black circles in FIG. 7) and graphite rings/sleeves (marked with the middle and outer black circles in FIG. 7) thermal neutron fluxes are lower. The absorption of the thermal neutrons in the fuel elements inside the fuel channel is also well described, indicating 18 zones (fuel elements, see FIG. 3) where thermal neutron fluxes are lowest.

The fast neutron distribution (FIG. 7 a)) is opposite to that of thermal neutron flux – most intensive fast neutron flux is in the regions of fuel elements inside the fuel channel, where uranium fuel fission takes place. Going further away from the fuel channel, fast neutron flux decreases and is lowest in the edges of modelled cell, due to neutron moderation in the graphite components. This moderation also determines the opposite distribution of the thermal neutrons – going further from the fuel channel, thermal neutron flux increases due to the thermalisation of fast (and resonance) neutrons. Radial distribution of resonance neutron flux (FIG. 7 b)) shows no significant distribution peculiarities, compared to the thermal or fast neutron fluxes, and intensity of the flux is almost the same in the radial direction in the graphite components, being slightly higher in the graphite rings/sleeves.

Neutron flux modelling results for the heights corresponding to the centres of top and bottom reflectors show different situation compared to the heights corresponding to the centres of the fuel bundles. The reflectors are situated away from the fuel bundles, thus neutron fluxes of all energies here are quite homogeneously distributed within graphite blocks and rings/sleeves. However, some features may also be observed on the neutron flux distributions in other structures than the graphite blocks or rings/sleeves. For the thermal flux distribution in the top reflector (FIG. 7 c)), the decrease in the central area inside the fuel channel is clearly described. Such phenomena here is caused due to the absorption of thermal neutrons in the extension rod of fuel assembly, which is made of stainless steel. Furthermore, for the resonance fluxes (FIG. 7 b)) in the top and bottom reflectors, the decrease is also observed in the area inside the fuel channel. This is mainly influenced by the interaction (moderation and absorption) of resonance neutrons with the coolant (water).

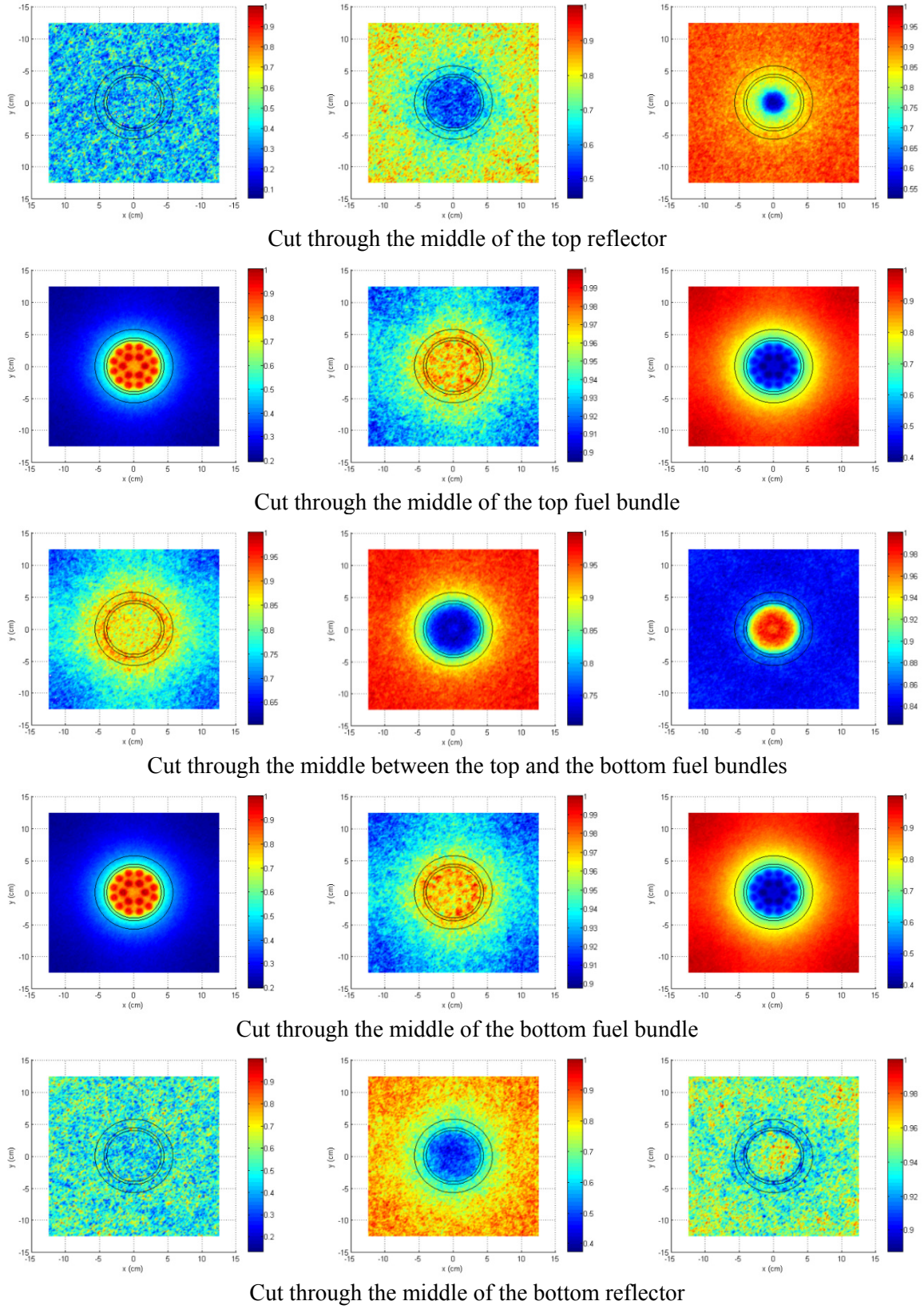

a) Fast b) Resonance c) Thermal

FIG. 7. Radial distribution of modelled neutron fluxes in the reactor RBMK-1500 one cell model at different heights.

Another situation is for the height corresponding to the axial centre of the active zone (centre between upper and lower fuel bundles). Thermal neutron flux is quite homogeneously distributed in the graphite rings/sleeves and blocks, but due to the additional thermalisation of higher energies neutrons within the coolant, it has an increase inside the fuel channel. For fast neutrons, the distribution shows an increase of neutron flux in the central area and decrease going further to the periphery of the modelled cell, i.e. fast flux is higher in the rings/sleeves than in graphite blocks. Resonance fluxes show similar behaviour as for top and bottom reflector cases.

The above presented radial distributions of neutron flux (FIG. 7) are useful for visualisation and interpretation of the results, but are not very useful for the neutron activation modelling.

3.1.1.2. Axial (longitudinal) distribution

Neutron fluxes presented in this 3.1.1.2 subchapter are averaged over the whole cross-section of each component in the lateral (radial) direction (and over the height of 50 cm in the axial direction) and indicate axial distribution of these laterally averaged fluxes in the particular graphite component.

Graphite blocks

The results of the neutron flux modelling show that the thermal and resonance neutron fluxes are dominant in the graphite column (blocks); however, the thermal neutron flux is more intensive than the resonance neutron flux (though very insignificantly in certain regions), see FIG. 8.

The fast neutron flux is about 10 times lower than that of resonance neutrons and their distribution along the axial direction is the same as the resonance neutron flux variation. As expected, there are two maximums and one minimum in the distribution profile of the fast and resonance neutron fluxes at the point in the reactor core, which corresponds to the point of the fuel bundles connection in the fuel assembly. In this region the fast and resonance neutron fluxes are ~1.2 times lower than their maximal values in the axial distribution. In the graphite column edges (reflector blocks) the fast and resonance neutron fluxes are ~34 (top reflector) and ~28 (bottom reflector) times lower than their maximal values in the axial distribution.

In case of thermal neutron flux there is only one maximum in the neutron flux distribution and it is located in the central part of the reactor core. Going further from the reactor core centre, the thermal flux decreases monotonically and in the graphite column edges i.e. top and bottom reflectors it is ~8 and ~6 times lower than the maximal flux value, respectively.

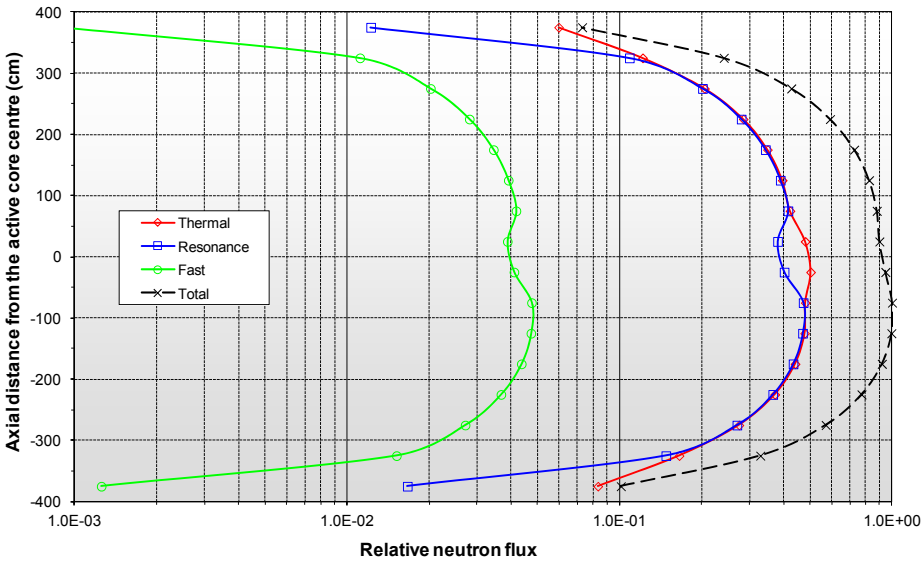

FIG. 8. Axial distribution of neutron fluxes in the graphite column.

Graphite rings/sleeves

Similar neutron flux distributions are obtained and for graphite rings/sleeves in the reactor core. The results of the neutron flux modelling show that the thermal and the resonance neutron fluxes are dominant in the graphite rings/sleeves and the fast neutron flux is about 6 times lower than that of resonance neutrons, as presented in FIG. 9.

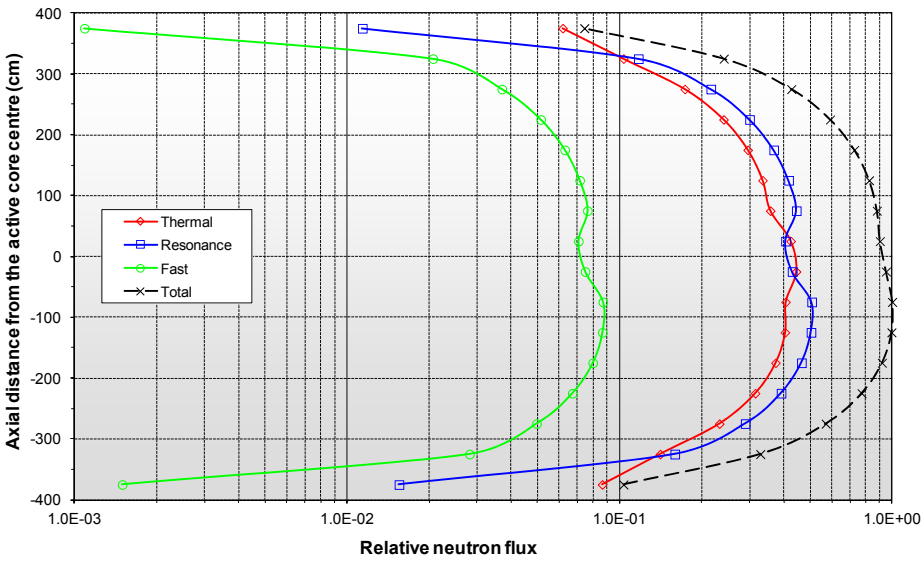

FIG. 9. Axial distribution of neutron fluxes in the graphite rings/sleeves.

However, in contrast to graphite blocks, the resonance neutron flux is more intense than the thermal neutron flux (except the very centre, the top and the bottom reflectors regions) in the graphite rings/sleeves.

Comparison of neutron fluxes in the graphite blocks and rings/sleeves (see FIG. 8 and FIG. 9) gives that distribution profiles of each energy group neutron fluxes are similar for both graphite components. However, while resonance neutron flux intensities are almost equal in these structures, the intensity of thermal neutron flux is higher in the graphite blocks than in rings/sleeves, whereas intensity of fast neutron flux is lower in the graphite blocks than in graphite rings/sleeves.

3.1.1.3. Spatial (lateral + longitudinal) distribution of neutron fluxes

Neutron fluxes presented in this 3.1.1.3 subchapter are averaged over the cross-section of each segment of the graphite component in the lateral (radial) direction (and over the heights of 50 cm in the axial direction) and thus indicate spatial (axial + radial) distribution of neutron fluxes in the particular graphite component.

Definitions “Inner”, “Middle” and “Outer” here stand for neutron fluxes obtained in the inner segment, middle segment and outer segment of the graphite blocks or rings/sleeves, as described in 2.2 subchapter.

Graphite blocks

The results of modelled neutron fluxes in the three segments of graphite blocks are presented in FIG. 10 (a) – Thermal flux, b) – Resonance flux, c) – Fast flux, d) – Total flux).

The achieved results show that neutron flux variation values for each of energy group are the same for all three graphite blocks segments and, as it could be expected, thermal neutron flux increases going away from inner segment to the outer, whereas the fast neutron flux decreases. The average difference

(along the height of the graphite blocks) between the thermal neutron fluxes (FIG. 10 a)) in the inner and the outer segments is ~10 %, while for the fast neutron fluxes (FIG. 10 c)) this difference is ~28 %. This means that on the average, the thermal neutron flux in the outer segment of graphite blocks is ~1.1 times higher than the flux in the inner segment, whereas the fast neutron flux is ~1.3 times higher in the inner segment of graphite blocks. The fluxes of the fast and thermal neutrons in the middle segment of graphite blocks are in-between the respective neutron fluxes of the inner and outer segments.

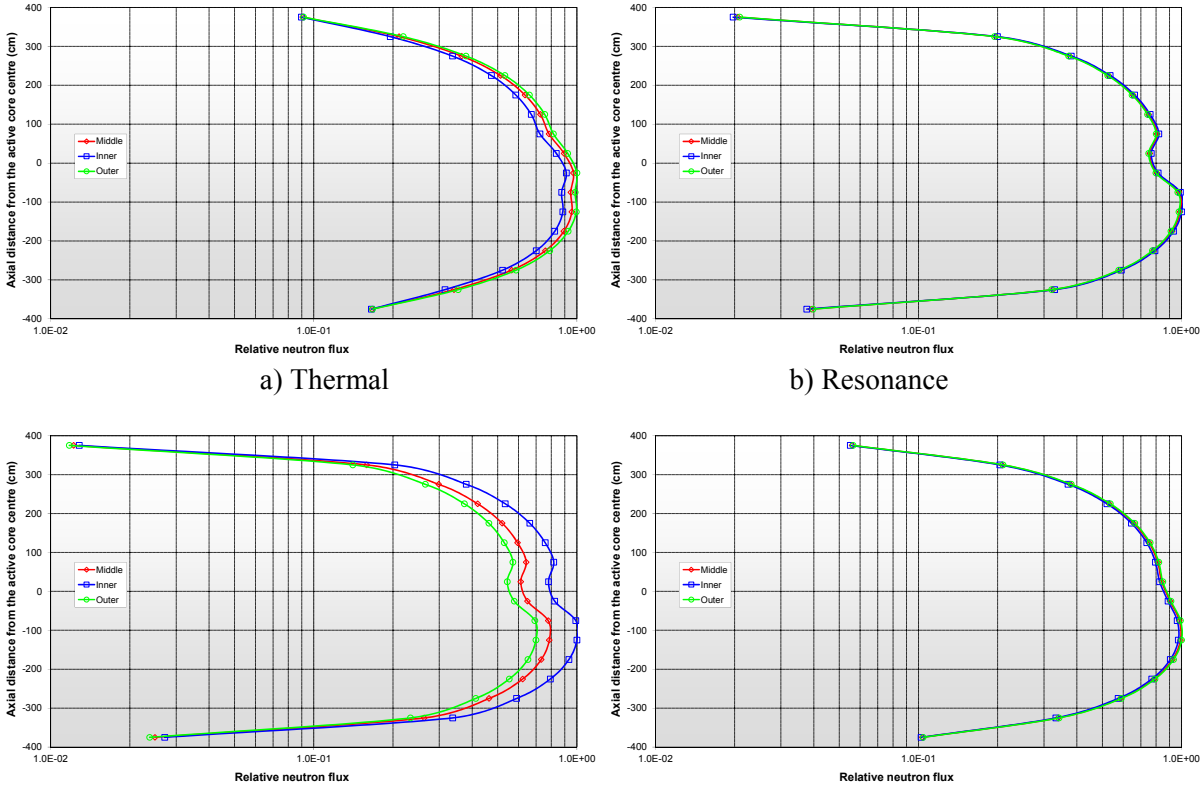

FIG. 10. Spatial distribution of neutron fluxes in the graphite blocks.

The differences of resonance (FIG. 10 b)) and total (FIG. 10 d)) neutron fluxes in the three segments of graphite blocks are quite small and average difference (along the height of graphite blocks) for both fluxes is only ~3 %.

Graphite rings/sleeves

An analogous situation is observed and for the segments of graphite rings/sleeves in the reactor core, as presented in FIG. 11. The differences here are even less, because graphite rings/sleeves are of much smaller dimensions in radial direction compared to the graphite blocks.

The average difference (along the height of graphite rings/sleeves) between the thermal neutron fluxes (FIG. 11 a)) in the inner and outer segments of the graphite rings/sleeves is ~6 %, while for the fast neutron fluxes (FIG. 11 c)) this difference is ~14 %. This means that on the average, the thermal neutron flux in the outer segment of graphite rings/sleeves is up to 1.1 times higher than the flux in the inner segment, whereas the fast neutron flux is up to 1.2 times higher in the inner segment of rings/sleeves. The fluxes of fast and thermal neutrons in the middle segment of graphite rings/sleeves are in-between the respective neutron fluxes of the inner and outer segments.

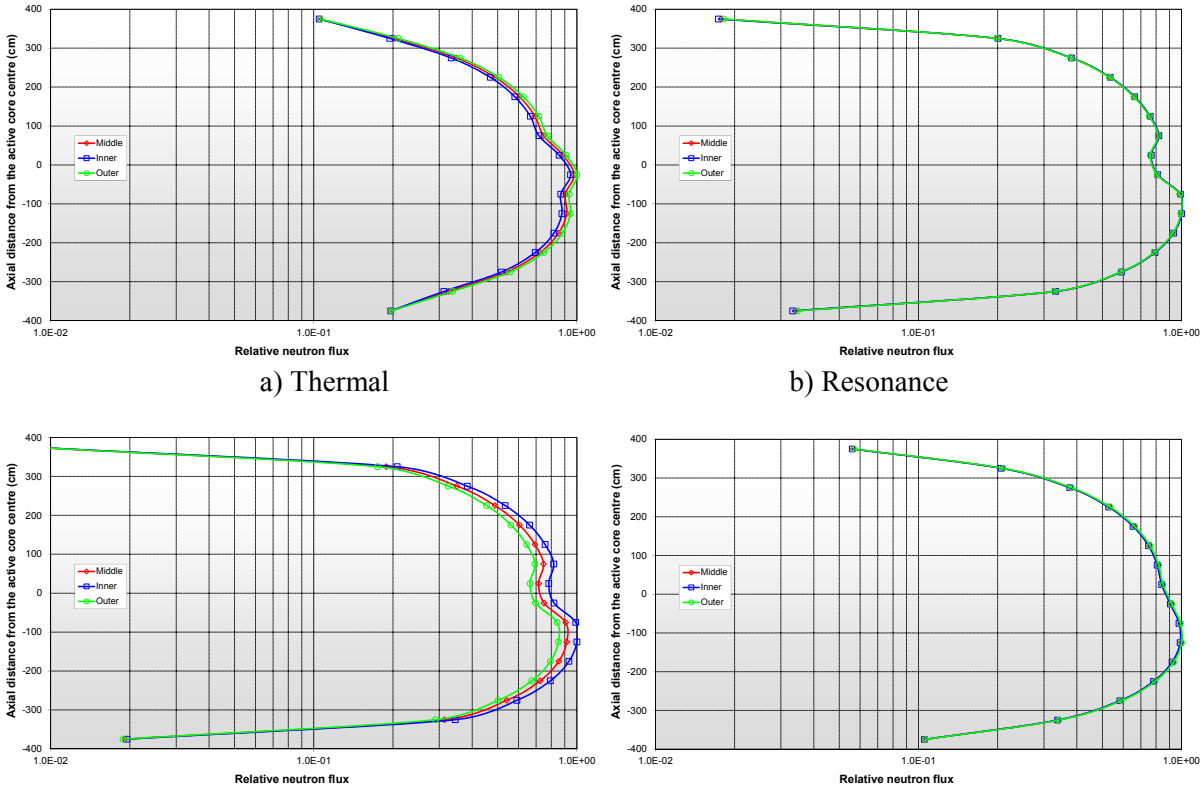

FIG. 11. Spatial distribution of neutron fluxes in the graphite rings/sleeves.

The differences of resonance (FIG. 11 b)) and total (FIG. 11 d)) neutron fluxes in the three segments of graphite blocks are very small and average difference (along the height of graphite rings/sleeves) for both fluxes is only up to 2 %.

3.1.2. Impact of fuel types on modelled neutron flux

It was already mentioned, that three different cases of one cell model were developed to analyse the impact of nuclear fuel type and burnup on the distributions of the modelled neutron fluxes in the RBMK-1500 reactor graphite components.

Definitions “2.4 Er burn”, “2.4 Er fresh” and “2.0 fresh” here stand for neutron fluxes obtained using different assumptions on the fuel, i.e. irradiated fuel with erbium, fresh fuel with erbium and fresh fuel without erbium, respectively, as described in 2.2 subchapter.

3.1.2.1.Graphite blocks

The modelling results for graphite blocks obtained for these three different fuel cases are presented in FIG. 12 (a) – Thermal flux, b) – Resonance flux, c) – Fast flux, d) – Total flux).

As presented in FIG. 12 a), the most intensive thermal neutron flux along the axial direction (except the central part and edges) is obtained using the model where fresh fuel without erbium absorber was assumed (comparing all three cases). Minimal differences of thermal neutron flux density are obtained in the centre and edges (~4 % and ~6 %, respectively), while the largest differences are obtained in the in-between parts (maximal difference of ~12 % is located 275 cm below the core centre). The average difference along the height of graphite blocks column is about 7 % and neutron fluxes variation characters are generally the same except the central part for fresh fuel without erbium. The comparison of the neutron flux distributions obtained using the fresh and irradiated fuel with erbium absorber (“2.4 Er fresh” and “2.4 Er burn”) shows, that the maximal differences are obtained in the centre and at the

edges (~4 % and ~6 %, respectively), whereas in the other parts the differences between the fluxes are smaller (up to 3 %). Such a variation of neutron fluxes confirms the fact, that the presence of burnable erbium absorber in the nuclear fuel decreases the maximal power of fresh uranium-erbium fuel assemblies, as the thermal neutron flux decreases due to the additional absorption in erbium. Due to the erbium burnup, the power of uranium-erbium fuel assemblies varies less during the operation than that of usual uranium fuel assemblies. The lower differences between the power of the fuel assemblies with different burnup determine better (more even) power distribution within the reactor core.

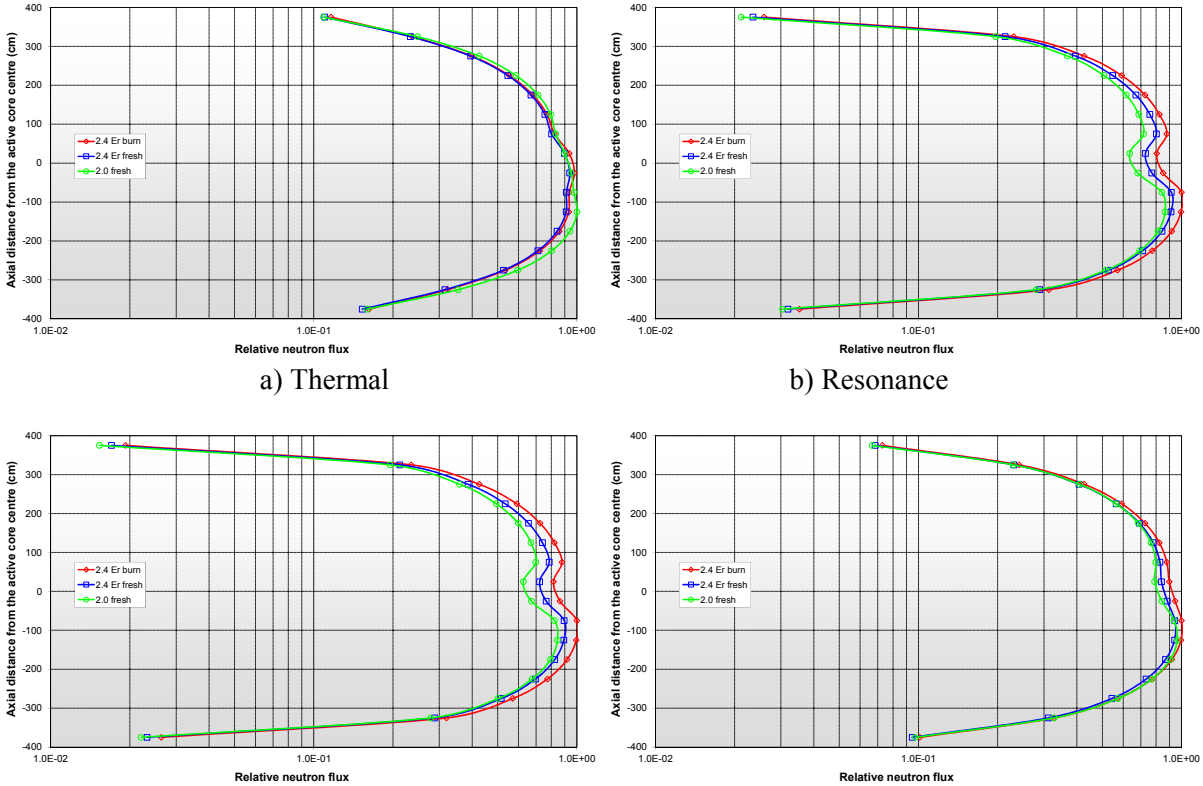

FIG. 12. Distribution of neutron fluxes in the graphite blocks (dependence on fuel types).

Results for resonance and fast neutron fluxes are presented in FIG. 12 b) and FIG. 12 c) respectively. The most intensive resonance and fast neutron fluxes along the axial direction are obtained using the model where irradiated fuel with erbium absorber was assumed ("2.4 Er burn"). Minimal differences of resonance and fast neutron flux densities are ~10 % and ~12 %, respectively, while the largest differences are ~21 % and ~23 %. The average difference along the height of graphite blocks column is ~15 % for the resonance flux and ~17 % for the fast neutron flux. Neutron flux variation values are the same for all cases. The highest resonance and fast neutron fluxes are obtained for the "2.4 Er burn" case and the lowest – for "2.0 fresh" case.

Comparison of total neutron fluxes (see FIG. 12 d)), shows that the differences are similar to those of the thermal neutron fluxes. Minimal difference of total neutron flux density is about ~4 %, while the maximal difference is about ~12 %. The average difference along the height of the graphite column is about 7 % and neutron fluxes variation characters are similar.

3.1.2.2.Graphite rings/sleeves

Very similar neutron flux distributions are obtained and for the graphite rings/sleeves in the reactor core, as presented in FIG. 13. The most intensive thermal neutron flux along the axial direction (except the centre and edges) is obtained using the model where fresh fuel without erbium absorber was assumed (comparing all three cases), see FIG. 13 a). Minimal differences of thermal neutron flux

densities are obtained in the centre and edges (~3 % and ~6 %, respectively), while the largest differences are obtained in the in-between parts (maximal difference of ~14 % is located 275 cm below core centre). The average difference along the height of graphite rings/sleeves is about 9 % and neutron flux variation values are generally the same except the central part for the fresh fuel without erbium. The comparison of the neutron flux distributions obtained using the fresh and irradiated fuel with erbium absorber ("2.4 Er fresh" and "2.4 Er burn") show, that the maximal differences are obtained in the centre and at the edges (~3 % and ~6 %, respectively), whereas in the other parts the differences of the fluxes are smaller (up to 2 %).

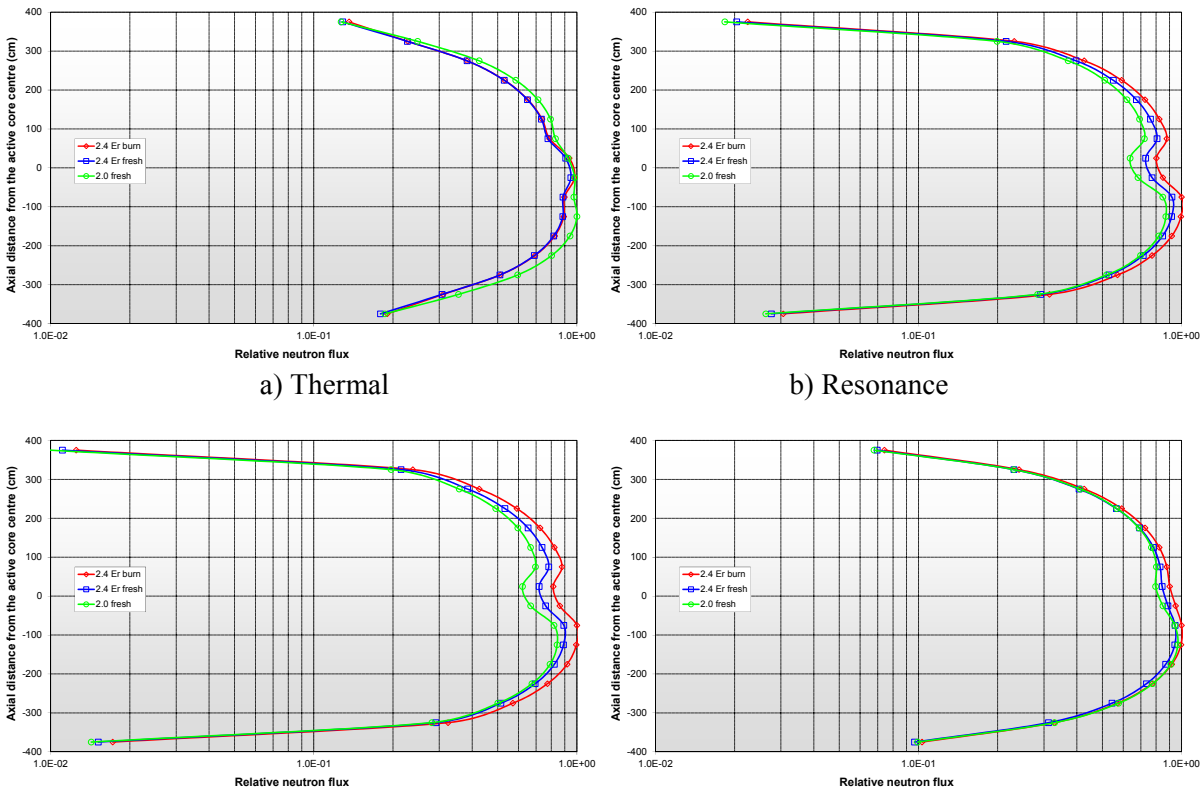

FIG. 13. Distribution of neutron fluxes in the graphite rings/sleeves (dependence on fuel types).

Results for resonance and fast neutron fluxes are presented in FIG. 13 b) and FIG. 13 c) respectively. The most intensive resonance and fast neutron fluxes along the axial direction are obtained using the model where irradiated fuel with erbium absorber was assumed ("2.4 Er burn"). Minimal differences of resonance and fast neutron flux densities are ~9 % and ~12 %, respectively, while the largest differences are ~21 % and ~24 %. The average difference along the height of graphite rings/sleeves is ~14 % for resonance flux and ~17 % for fast neutron flux. Neutron flux variations are the same for all cases, and the highest resonance ant fast neutron fluxes are obtained for the "2.4 Er burn" case, while the lowest – for "2.0 fresh" case.

Comparison of total neutron fluxes (see FIG. 13 d)), shows that the differences are similar to those of thermal neutron fluxes. Minimal difference of total neutron flux density is about ~4 %, while the maximal difference is about ~12 %. The average difference along the height of the graphite rings/sleeves is about 7 % and neutron flux variation character is similar.

3.1.3. Impact of nuclear data libraries on modelled neutron fluxes

The impact of different data libraries on modelled neutron fluxes was also evaluated. Three different nuclear data libraries from MCNP 6 package (ENDF/B-V, ENDF/B-VI and LLNL) were selected for the evaluation of the different data libraries impact on the modelled neutron fluxes (see 2.2

subchapter). Definitions “ENDF/B-VI”, “ENDF/B-V” and “LLNL” here stand for neutron fluxes obtained using different nuclear data libraries for the neutron transport modelling, i.e. Evaluated Nuclear Data File (ver. VI), Evaluated Nuclear Data File (ver. V) and Lawrence Livermore National Laboratory nuclear data library.

3.1.3.1. Graphite blocks

The results for graphite blocks on the influence of the different nuclear data libraries for the modelled neutron fluxes are presented in FIG. 14 (a) – Thermal flux, b) – Resonance flux, c) – Fast flux, d) – Total flux).

The achieved results show that there is no significant influence of these analysed data libraries on the modelled neutron fluxes in the graphite blocks. The neutron flux variation characeristics for each of the energy groups are the same using all three data libraries. The average differences along the height of graphite blocks column are only ~7 % for fast (FIG. 14 c)), ~3 % for resonance (FIG. 14 b)) and ~2 % for thermal (FIG. 14 a)) and total (FIG. 14 d)) neutron fluxes.

The maximal difference of modelling results for thermal neutron fluxes (FIG. 14 a)) using mentioned data libraries is ~5 %, while minimal is less than 1 %. Analogous situation is for total neutron fluxes (FIG. 14 d)) where maximal difference is even lower – ~4 %, and minimal is also less than 1 %.

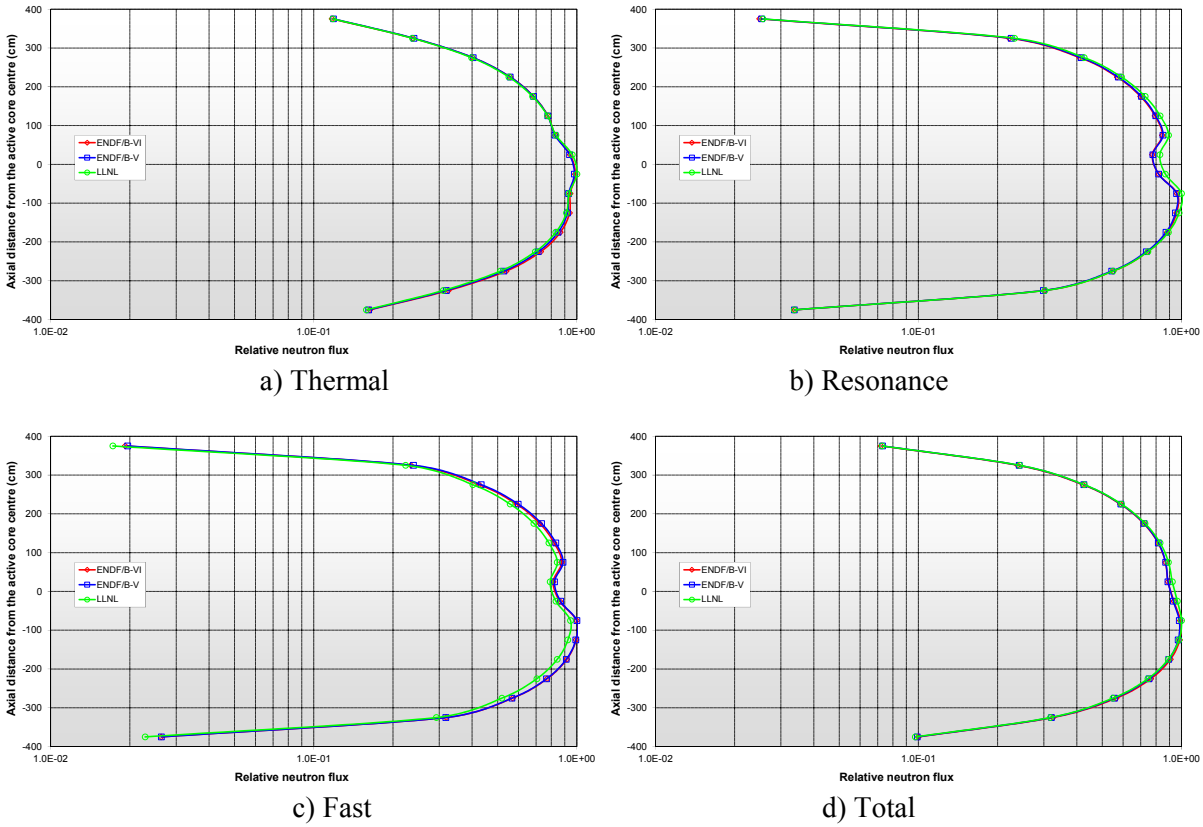

FIG. 14. Distribution of neutron fluxes in the graphite blocks (dependence on data libraries).

For resonance (FIG. 14 b)) and fast (FIG. 14 c)) neuron fluxes these differences are slightly higher – maximal differences are ~6 % and ~13 %, while the minimal are less than 1 % and ~4 %, respectively.

3.1.3.2. Graphite rings/sleeves

Very similar neutron fluxes distributions are obtained and for graphite rings/sleeves in the reactor core, as presented in FIG. 15. The achieved results show that there is no significant influence of these

analysed data libraries on the modelled neutron fluxes in graphite rings/sleeves. The neutron fluxes variation characters for each of the energy group is the same using all three data libraries. The average differences along the height of graphite rings/sleeves are only ~4 % for fast (FIG. 15 c)) and for resonance (FIG. 15 b)) fluxes, and ~2 % for thermal (FIG. 15 a)) and total (FIG. 15 d)) neutron fluxes.

The maximal difference of modelling results for thermal neutron fluxes (FIG. 15 a)) using the identified data libraries is ~5 %, while minimal is less than 1 %. Analogous situation is for total neutron fluxes (FIG. 15 d)), where maximal difference is even lower – ~4 %, and minimal is a bit higher – ~1 %. For resonance (FIG. 15 b)) and fast (FIG. 15 c)) neuron fluxes these differences are slightly higher – maximal differences are ~7 % and ~11 %, respectively, while minimal differences are less than 1 %.

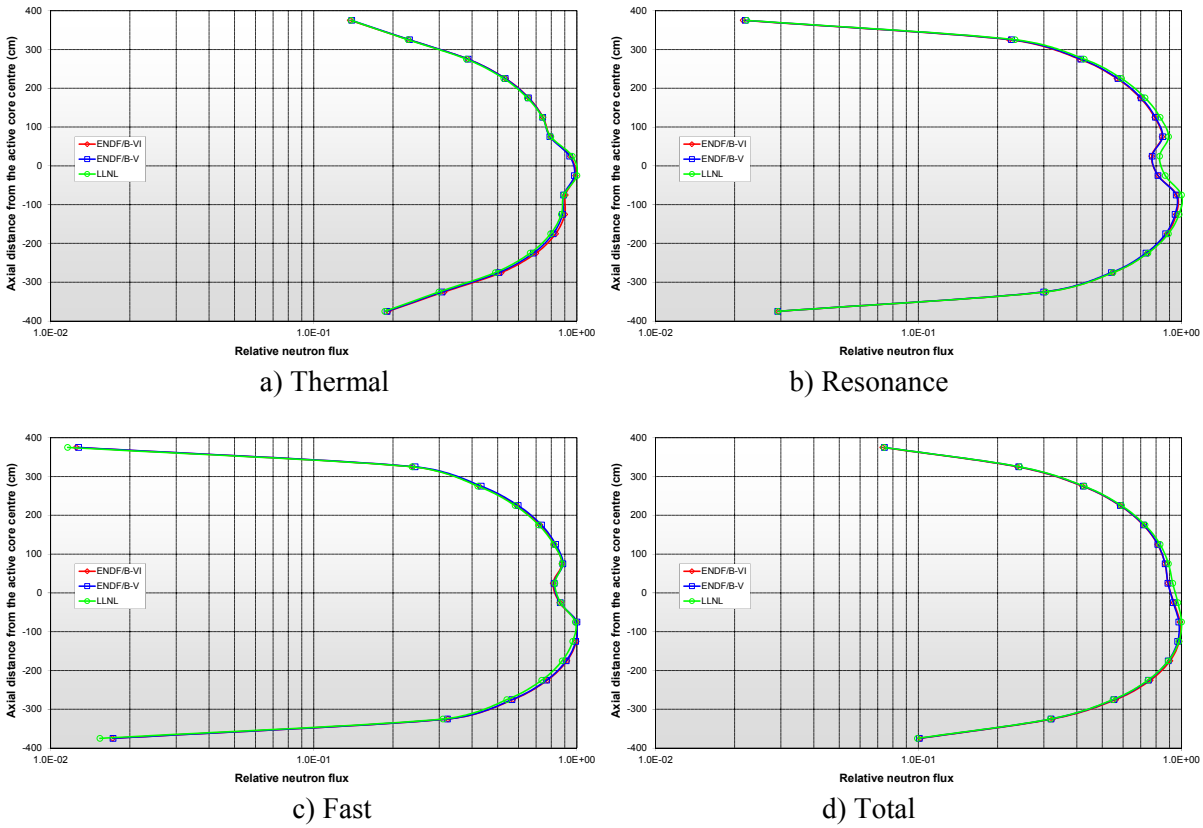

FIG. 15. Distribution of neutron fluxes in the graphite rings/sleeves (dependence on data libraries).

3.2. Neutron induced activities in graphite components

In all cases of subsections 3.2.1, 3.2.2 and 3.2.3, when performing the neutron activation modelling, the activity variation in the axial direction in the analysed graphite component was assessed and radionuclides emerging in the activated material, as well as their radioactivity levels, were evaluated at the time just after the irradiation termination (i.e. at the time of the reactor final shutdown – RFS), and for several decay (cooling) periods after the irradiation termination, i.e. after RFS.

The list of nuclides for the graphite blocks, presented in FIG. 17 and FIG. 19, is selected in the way that only those nuclides, whose specific activities after 2 years cooling are not less than 1×10^{-3} % of the total specific activity at RFS, are accounted. For graphite rings/sleeves (FIG. 21 and FIG. 23) this threshold activity level was set to 5×10^{-3} %, as they have more short-lived nuclides (due to the longer list of reported initial impurities) which encumber visualization. In order to ease comparison of specific activities of particular radionuclide for the minimal and maximal initial impurities concentration cases, the lists of radionuclides in FIG. 25 and FIG. 28 are the same as for FIG. 19 and FIG. 23, respectively.

3.2.1. Graphite blocks

3.2.1.1. Unit 1

Using the maximal concentration of impurities, modelled total specific activity of the graphite blocks of Unit 1 reactor within the top reflector, active zone and bottom reflector is quite even distributed at the time of RFS ((1.0 – 1.4)×10^8 Bq/g), see FIG. 16. Specific activity decreases ~1.5 times during 5 years, but the distribution profile stays very similar. The maximal activity is observed in the graphite blocks of the reactor core centre, but the distribution profile is different from the distribution profiles of the neutron fluxes – i.e. total specific activity of the top and bottom reflector blocks are respectively only ~1.3 and ~1.2 times lower than the maximal activity of the active core blocks (FIG. 8).

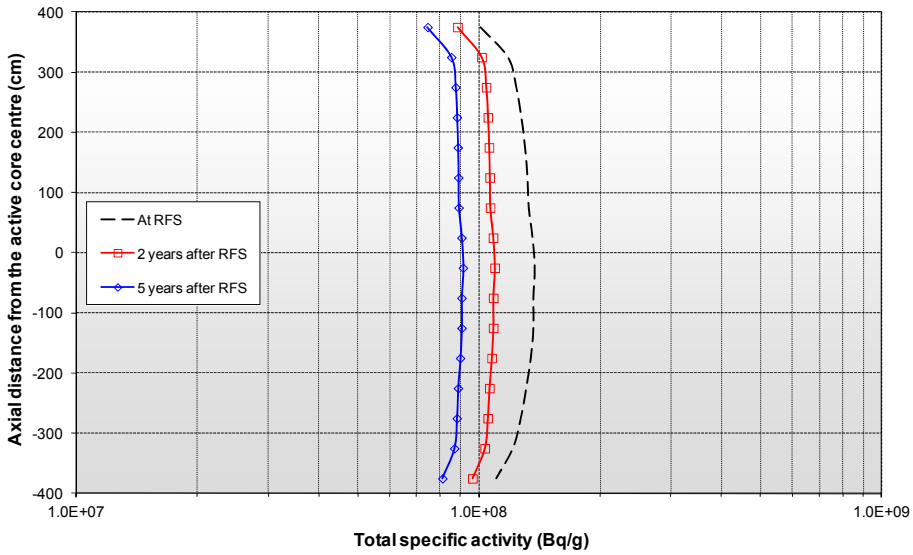

FIG. 16. Axial distribution of the graphite blocks total specific activity and its variation during 5 years after RFS (Unit 1, max. imp. conc.).

The principal radionuclides and their average (averaged over the height of reactor core) activity variation in the graphite blocks of Unit 1 reactor are presented in FIG. 17.

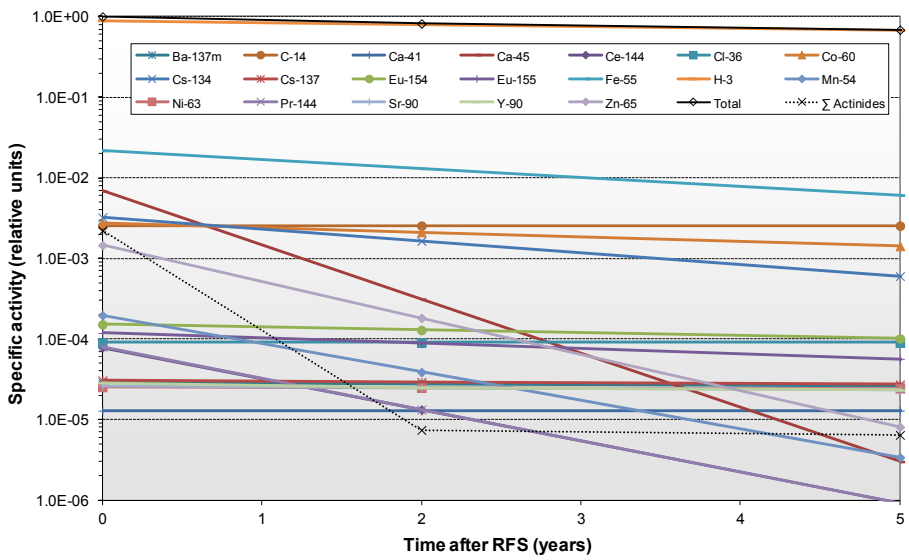

FIG. 17. Principal radionuclides and their activity variation in the graphite blocks during 5 years after RFS (Unit 1, max. imp. conc.).

H-3, Fe-55, Co-60, C-14 and Cl-36 are the most important nuclides in the graphite blocks during 5 cooling years from the activity point of view. Total specific activity is determined by the short-lived H-3 and Fe-55 during 5 years after RFS, while C-14 has the highest activity among the long-lived.

3.2.1.2. Unit 2

A similar situation is observed for the Ignalina NPP Unit 2 reactor graphite blocks, but the induced activities are slightly higher. Total specific activity of the graphite blocks within the top reflector, active core and bottom reflector is quite even distributed at the time of RFS ($(1.1 – 1.4)\times10^8$ Bq/g), see FIG. 18. It decreases about 1.5 times after 5 cooling years, but the distribution profile stays almost identical. The maximal activity is observed in the graphite blocks of the reactor core centre; total specific activities of top and bottom reflector blocks are respectively only ~1.3 and ~1.2 times lower.

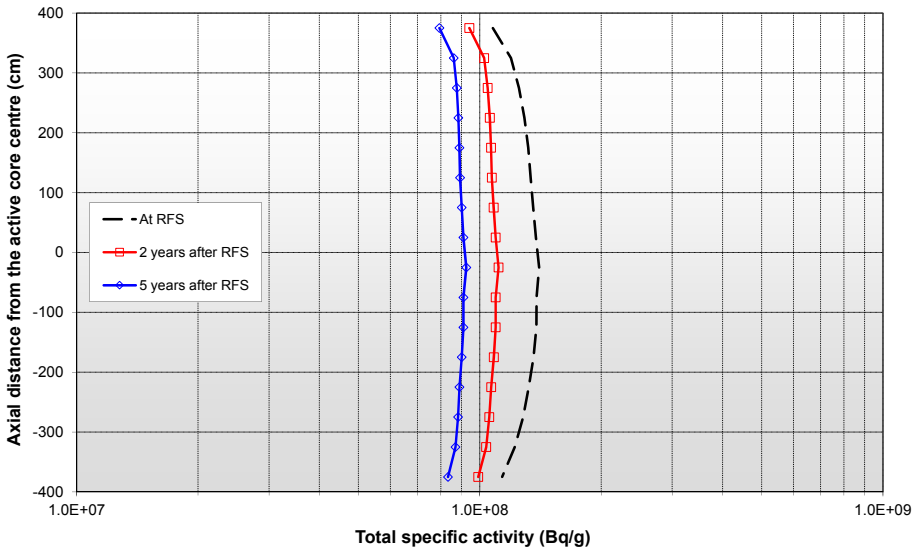

FIG. 18. Axial distribution of the graphite blocks total specific activity and its variation during 5 years after RFS (Unit 2, max. imp. conc.).

FIG. 19 presents the main nuclides and their average activity variation in the graphite blocks of Unit 2.

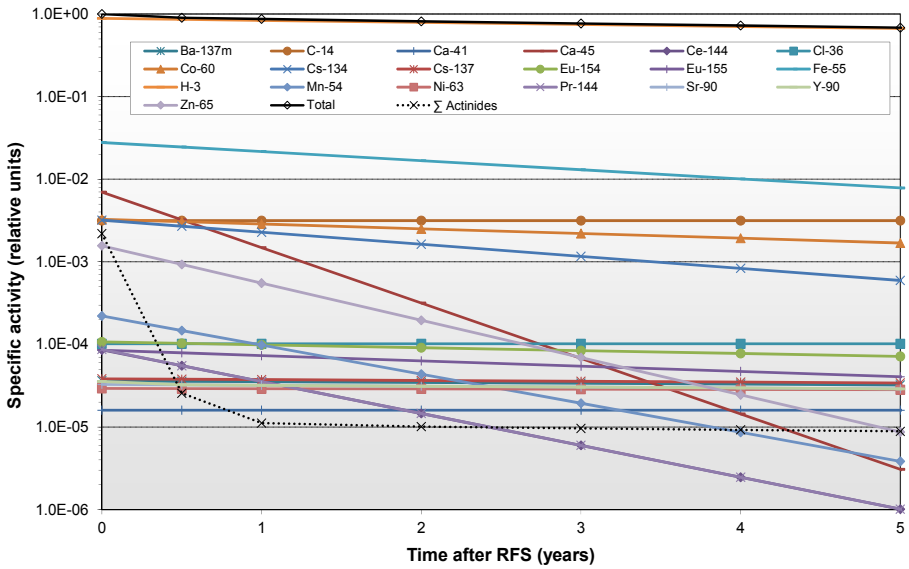

FIG. 19. Principal radionuclides and their activity variation in the graphite blocks during 5 years after RFS (Unit 2, max. imp. conc.).

The most important radionuclides in the graphite blocks of Unit 2 during 5 cooling years from the activity point of view are the same as for Unit 1. Total specific activity is determined by H-3 and Fe-55 during analysed cooling time, while C-14 has the highest activity among the long-lived nuclides.

3.2.2. Graphite rings/sleeves

3.2.2.1. Unit 1

The modelling results (FIG. 20) show that total specific activity distribution along the axial direction in the graphite rings/sleeves of Unit 1 reactor (in the top reflector, active core and bottom reflector) is almost identical to the thermal neutron flux distribution, see FIG. 9.

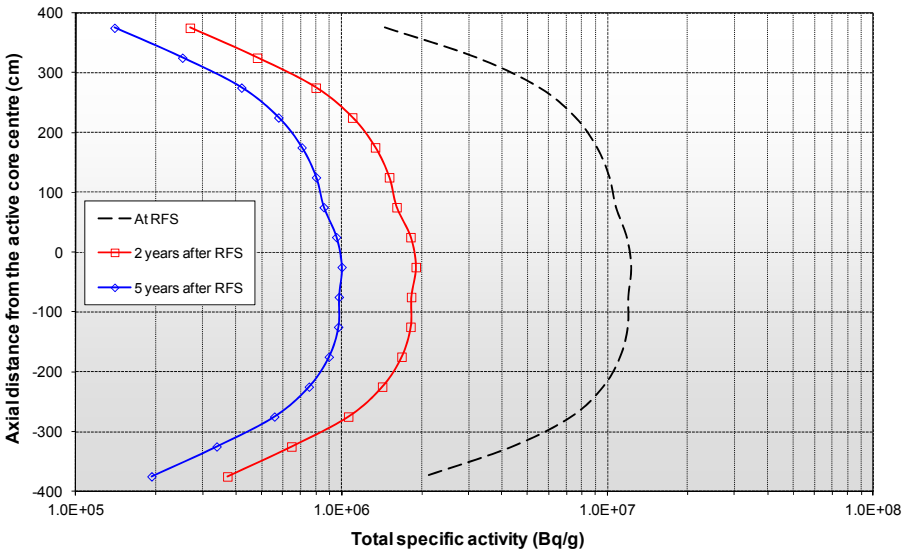

FIG. 20. Axial distribution of the graphite rings/sleeves total specific activity and its variation during 5 years after RFS (Unit 1, max. imp. conc.)

Total specific activity of the top and bottom reflector rings/sleeves are respectively ~8 and ~6 times lower than the maximal activity in the active core rings/sleeves (1.2×10^7 Bq/g at RFS). The distribution profile stays almost identical during 5 cooling years, but activity decreases ~12.5.

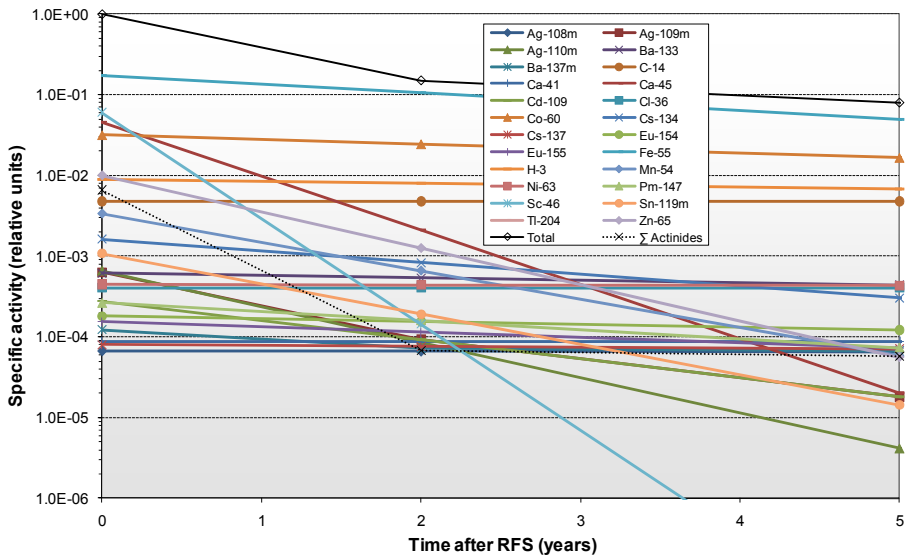

FIG. 21. Principal radionuclides and their activity variation in the graphite rings/sleeves during 5 years after RFS (Unit 1, max. imp. conc.).

Similarly to Unit 1 graphite blocks, radionuclides H-3, Fe-55, Co-60, C-14 and Cl-36 have highest specific activities, see FIG. 21 and FIG. 17. However, the total specific activity of the graphite rings/sleeves is determined by Fe-55 and Co-60, whereas for the graphite blocks H-3 was dominant.

3.2.2.2. Unit 2

The modelling results for Unit 2 graphite rings/sleeves are similar to those of Unit 1. Axial distribution of total specific activity is almost identical to the thermal neutron flux distribution (see FIG. 9), having one maximum at the active zone centre and two minimums in the reflectors, as presented in FIG. 22.

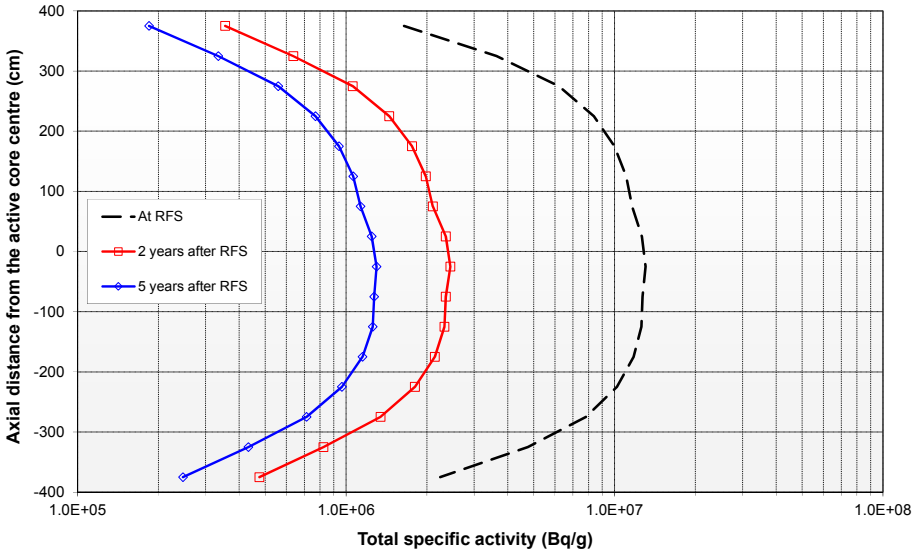

FIG. 22. Axial distribution of the graphite rings/sleeves total specific activity and its variation during 5 years after RFS (Unit 2, max. imp. conc.).

The maximal specific activity in the Unit 2 active zone graphite rings/sleeves is ~1.3×10^7 Bq/g at RFS, while specific activities in the top and bottom reflectors are respectively ~8 and ~6 times lower. Similarly to Unit 1, the distribution profile of total activity in the Unit 2 graphite rings/sleeves stays almost identical during 5 cooling years, but the activity itself decreases about 10.3 times, see FIG. 22.

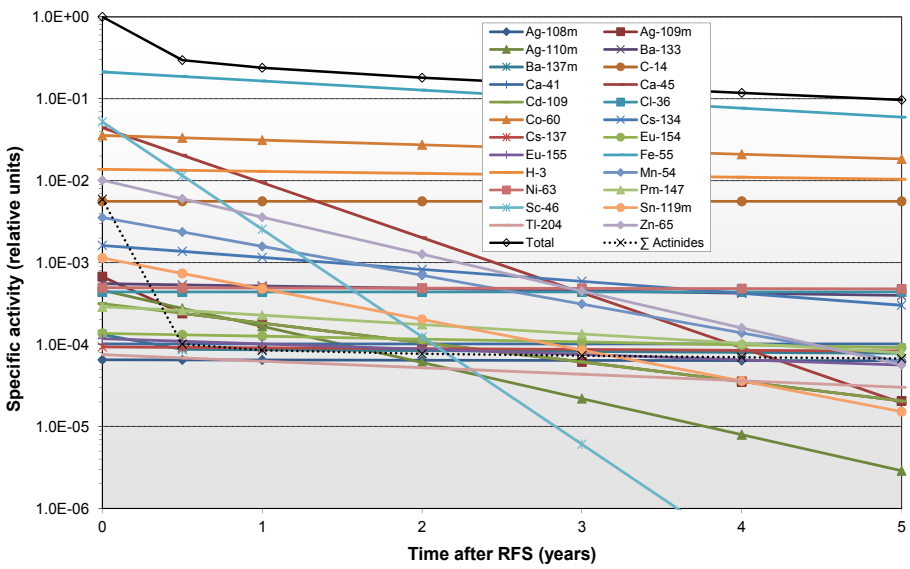

FIG. 23. Principal radionuclides and their activity variation in the graphite rings/sleeves during 5 years after RFS (Unit 2, max. imp. conc.).

The most important nuclides (having highest activities during 5 years cooling period) in the activated graphite rings/sleeves of Unit 2 are presented in FIG. 23. Analogous to Unit 1 graphite rings/sleeves, they are Fe-55, Co-60, H-3 (short-lived) and C-14, Cl-36 (long-lived) and total specific activity of graphite rings/sleeves is determined by Fe-55 and Co-60 (FIG. 23).

3.2.3. Impact of impurities concentrations on induced activities

The assessment of impact of different initial impurities concentrations on the modelled specific activities in the graphite blocks and rings/sleeves was made for Unit 2 reactor components. It was already mentioned, that for this purpose modelling of the induced activities was performed using minimal impurities concentrations for both grade graphites and taking into account Ignalina NPP Unit 2 reactor operation history.

For the convenience purposes, results obtained using minimal initial impurities concentrations and presented in this 3.2.3 subchapter are referred as results of the "non conservative case". In opposite, the results obtained using maximal initial concentrations of impurities, presented in subchapters 3.2.1 and 3.2.2, are called as results of the "conservative case".

3.2.3.1. Graphite blocks

In this non-conservative case, the distribution of the total specific activity along the height of graphite blocks column of Unit 2 reactor is not even, as presented in FIG. 24, and differs from the distribution profile obtained in the conservative case, see FIG. 18. At the time of the reactor final shutdown, the maximal specific activities are observed in the top and bottom reflectors blocks, where thermal neutron flux is lowest (see FIG. 8).

The maximal total specific activity of the top and bottom reflector graphite blocks is ~1.1×10^6 Bq/g, while for the active core graphite blocks it is ~8.5×10^5 Bq/g at the time of reactor final shutdown. After 5 cooling years period the total specific activities decrease approximately 5 times, keeping similar distribution profiles.

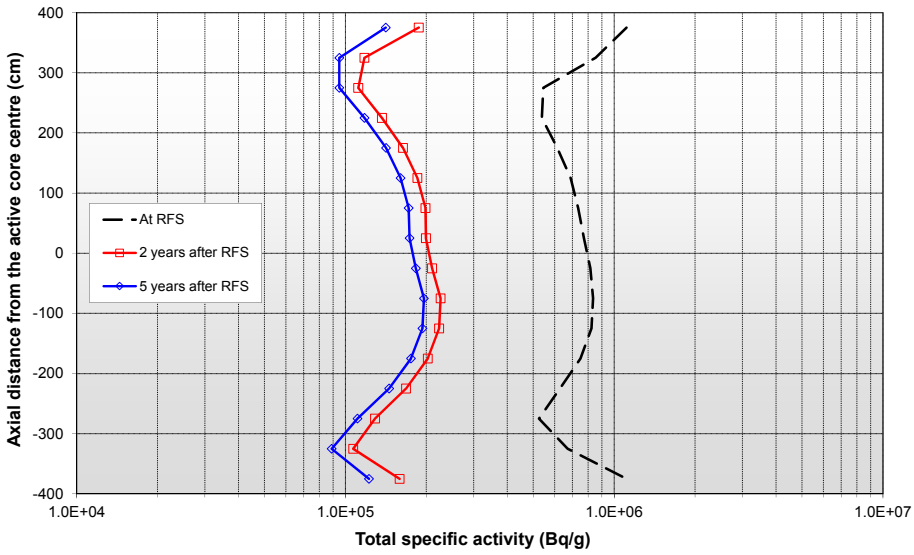

FIG. 24. Axial distribution of the graphite blocks total specific activity and its variation during 5 years after RFS (Unit 2, min. imp. conc.).

Similar to the conservative case, the most important nuclides (having highest specific activities) for this non conservative case are H-3, Co-60 and C-14 in the graphite blocks, however, contrary to the conservative case, Fe-55 and Cl-36 are not so important, see FIG. 25 and FIG. 19.

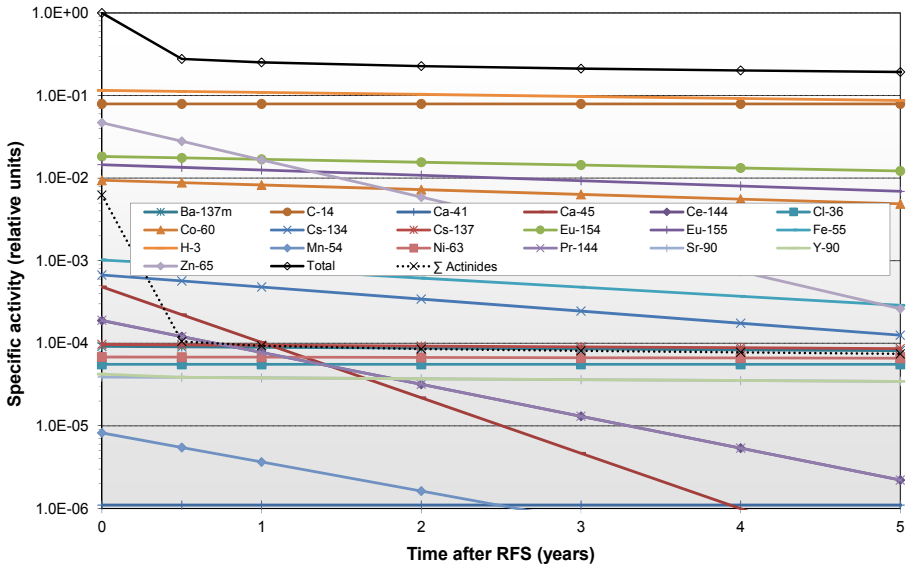

FIG. 25. Principal radionuclides and their activity variation in the graphite blocks during 5 years after RFS (Unit 2, min. imp. conc.).

For comparison purposes, FIG. 26 presents total specific activities and specific activities of selected radionuclides (averaged in the axial direction) in the graphite blocks for both modelling cases.

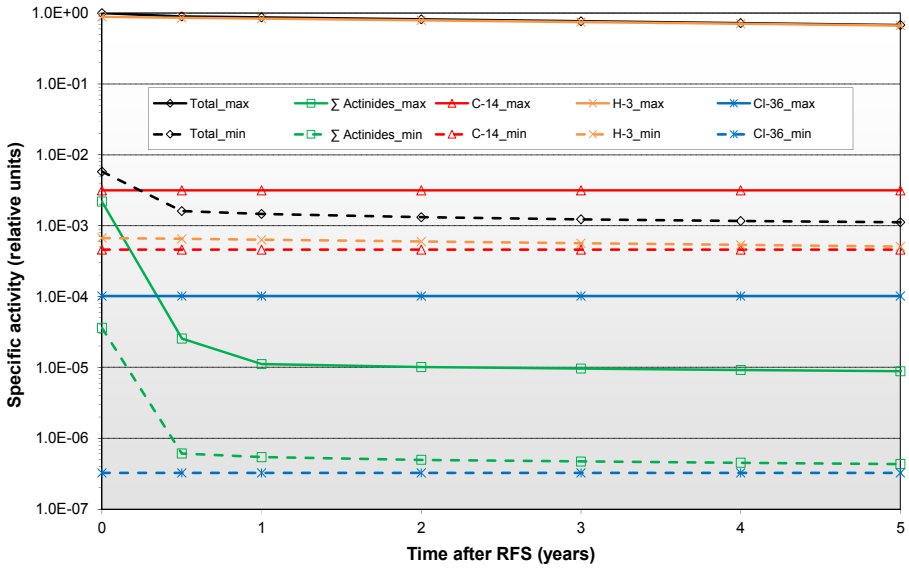

FIG. 26. Comparison of total and selected radionuclides specific activities variations in the graphite blocks during 5 years after RFS.

The definitions in the legend of FIG. 26 ending with "..._max" stand for specific activities obtained for the maximal impurities concentration (conservative) case, while definitions ending with "..._min" stand for specific activities obtained for the minimal impurities concentration (non conservative) case.

After the comparison of graphite blocks total specific activity axial distribution and its dependence on cooling time (FIG. 26) for conservative (FIG. 18) and non conservative (FIG. 24) cases, it is evident, that the differences of initial impurities concentrations have impact not only to the total specific activity, but also to its axial distribution profile as well as to the dependence on cooling time. This could be explained by the fact that in the active core of the reactor graphite stack, due to the intensive thermal neutron flux (or lower impurities concentrations) a part of impurities (mainly Eu in this particular case) just burns out, while in the regions with considerably lower thermal neutron fluxes (or

higher impurities concentrations) this process asserts not so significantly and this results in the different radionuclides and their activities content.

Average specific activities (averaged in the axial direction) of the entire column of graphite blocks at the RFS reach 1.3×10^{8} Bq/g and 7.5×10^{5} Bq/g for conservative and non conservative cases respectively, and after 5 cooling years these activities decrease to the ~8.8×10^{7} Bq/g and ~1.4×10^{5} Bq/g. So at RFS these average total specific activities differ almost 200 times for the maximal and minimal initial impurities concentrations cases and after 5 cooling years this difference increases up to 600 times.

This difference is determined mostly by the high differences of the initial concentrations of such impurities as Li, Fe and Co (differs more than 10^{3} times for Li and Fe and about 50 times for Co). For the conservative case, their activation products, namely H-3 and less significantly Fe-55 and Co-60, determines total specific activity of the active core graphite blocks. While for the non conservative case, only H-3 considerably influences total specific activity from the mentioned radionuclides, however its activity is still more than 10^{3} times lower than in the conservative case.

Regarding radionuclide C-14, it arises as activation product of the raw graphite material (carbon) and as activation product of the nitrogen impurity; however nitrogen impurity concentration in the conservative modelling case is more than 10^{2} times higher than that in the non conservative case, and thus the activity of C-14 is considerably higher for conservative modelling case.

3.2.3.2. Graphite rings/sleeves

In this non conservative case, the maximal specific activity of Unit 2 graphite rings/sleeves is lower than for conservative case and reaches ~3.7×10^{6} Bq/g at RFS. The axial distribution of the graphite rings/sleeves total specific activity is also not even, as presented in FIG. 27.

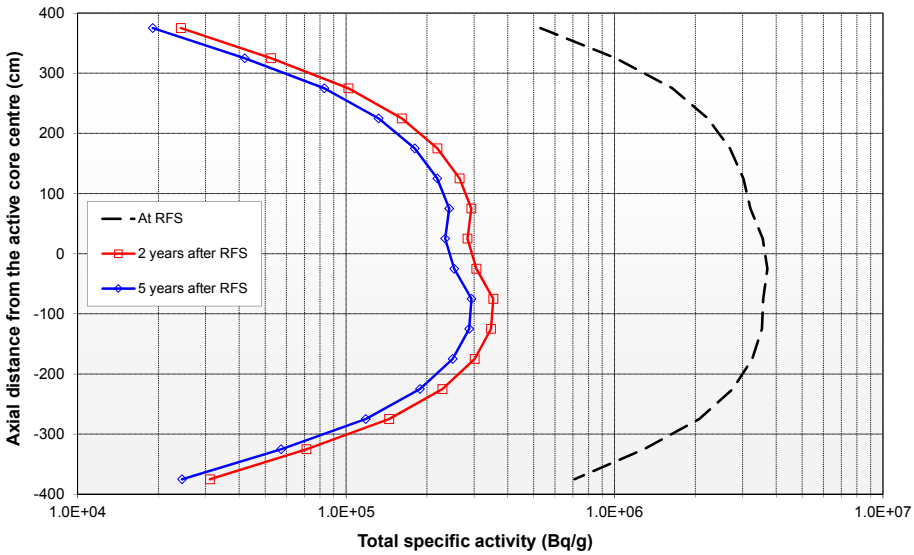

FIG. 27. Axial distribution of the graphite rings/sleeves total specific activity and its variation during 5 years after RFS (Unit 2, min. imp. conc.).

At RFS, the maximal total specific activity is in the central part of the active core where highest thermal neutron flux is observed, while total specific activities of the graphite rings/sleeves in the top and the bottom reflector regions are lower and minimal total specific activity of ~5.3×10^{5} Bq/g is in the top reflector. In other words, the axial distribution of total specific activity in the graphite rings/sleeves approximately corresponds to the thermal neutron flux distribution in these structures (see FIG. 9). During analysed 5 years after RFS, the maximal total specific activity of the active core

graphite rings/sleeves decreases to ~2.5×10^5 Bq/g, while total specific activity of the top reflector graphite rings/sleeves decreases to ~1.9×10^4 Bq/g (FIG. 27).

The most important nuclides (having highest specific activities) during the analysed 5 years cooling period in the graphite rings/sleeves are the same as for conservative case: the long-lived C-14, Cl-36 and short-lived H-3, Fe-55, and Co-60 (FIG. 28), however the activity of the last two radionuclides are several ten times lower than in the conservative case.

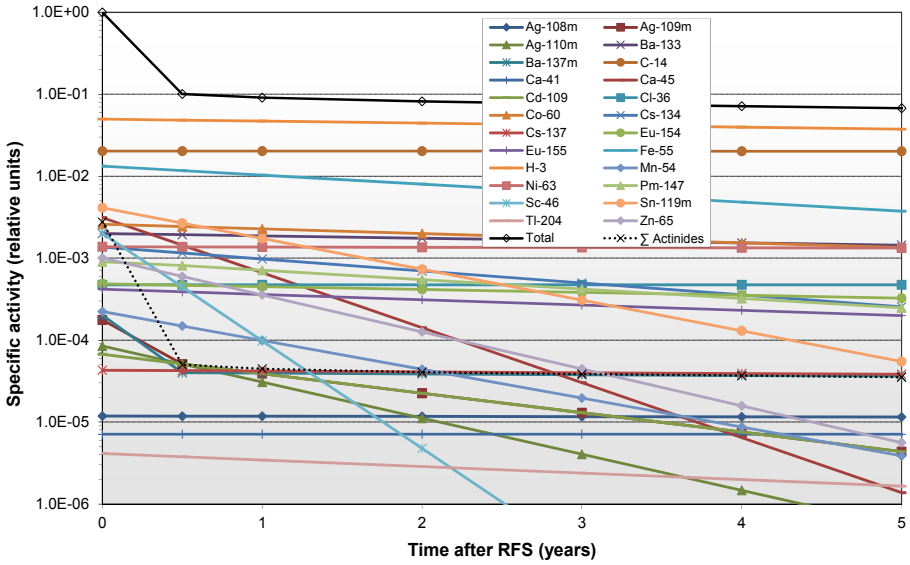

FIG. 28. Principal radionuclides and their activities variations in the graphite rings/sleeves during 5 years after RFS (Unit 2, min. imp. conc.).

For comparison purposes, FIG. 29 presents total specific activities and specific activities of selected radionuclides (averaged in the axial direction) in the graphite rings/sleeves for both modelling cases.

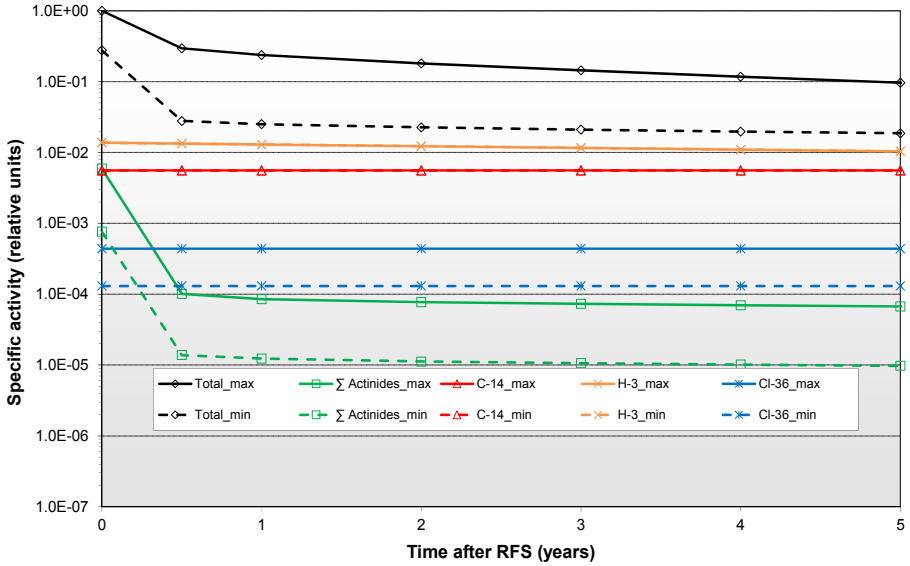

FIG. 29. Comparison of total and selected radionuclides specific activities variations in the graphite rings/sleeves during 5 years after RFS.

After the comparison of graphite rings/sleeves axial total specific activities distribution for the conservative (FIG. 22) and non conservative (FIG. 27) cases it is evident, that the differences of initial impurities concentrations have highest impact to the specific activities of active core graphite

rings/sleeves while differences of the specific activities for the top and bottom reflector graphite rings/sleeves are lower. This could be explained by the fact that in the active core of the reactor graphite stack, due to the intensive thermal neutron flux or lower impurities concentrations a part of impurities (such as Eu and others having large neutrons absorption cross-sections) just burns out, while in the regions with considerably lower thermal neutron fluxes (or higher impurities concentrations) they do not burn out completely.

Average (averaged in the axial direction) specific activity of the graphite rings/sleeves at the time of RFS reaches 8.8×10^6 Bq/g and 2.4×10^6 Bq/g for the conservative and non conservative cases respectively. So at RFS these activities differ ~3.6 times for the maximal and minimal initial impurities concentrations cases, but during 5 years after RFS this difference increases to ~5.2 times.

These differences of total specific activities are mainly determined by the differences of Fe-55 and Co-60 activities due to the different initial concentrations of Fe and Co impurities. For the conservative modelling case, Fe-55 and Co-60 comprise highest parts of the total specific activity.

For the non conservative case Fe-55 and Co-60 still are ones of the most active radionuclides at RFS, but their activities do not considerably influence the total specific activity which is determined by H-3 and C-14. As there is no data on Li and N impurities in the graphite rings/sleeves, the specific activities of C-14 and H-3 are the same for both modelling cases, i.e. C-14 arises from the activation of raw graphite material (carbon), whereas H-3 production is not affected by Li activation.

3.2.4. Spatial distribution of induced activities for selected radionuclides

To analyse the spatial distribution of the induced activities in the RBMK-1500 reactor graphite components, activation modelling was performed using neutron fluxes, obtained in 3.1.1.3 subchapter (FIG. 10 and FIG. 11), maximal initial impurities concentrations and Unit 2 reactor operation history.

Definitions “Inner”, “Middle” and “Outer” stand for different segments of the graphite components in the radial direction, as described in subchapter 2.2 and presented in FIG. 3 b).

3.2.4.1. Graphite blocks

The results of the induced activities for the different segments of the graphite blocks are presented in FIG. 30 – for H-3, FIG. 31 – C-14, FIG. 32 – Cl-36.

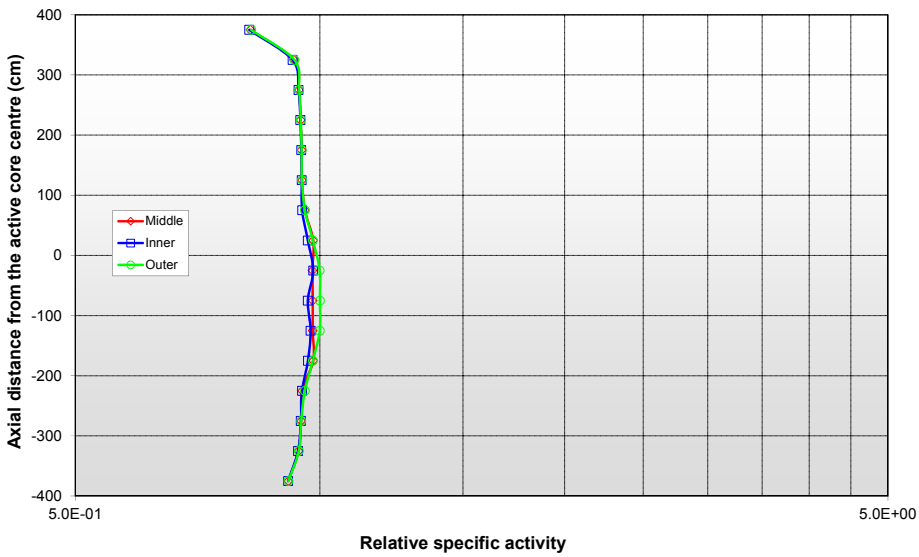

FIG. 30. Spatial distribution of H-3 specific activities in the different segments (see FIG. 3 b)) of the graphite blocks at RFS.

The achieved results show that there is no big difference of the induced activities of selected nuclides in the different segments of the graphite blocks. The variation character of specific activities for each radionuclide is the same in all segments. The average differences along the height of the graphite blocks are ~10 % for C-14 (FIG. 31), ~6 % for Cl-36 (FIG. 32) and less than 1 % for H-3 (FIG. 30).

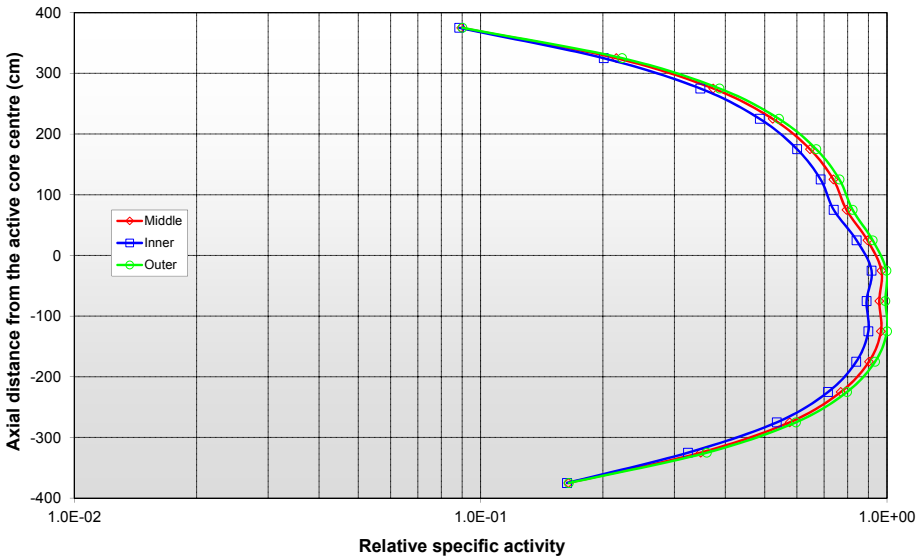

FIG. 31. Spatial distribution of C-14 specific activities in the different segments (see FIG. 3 b)) of the graphite blocks at RFS.

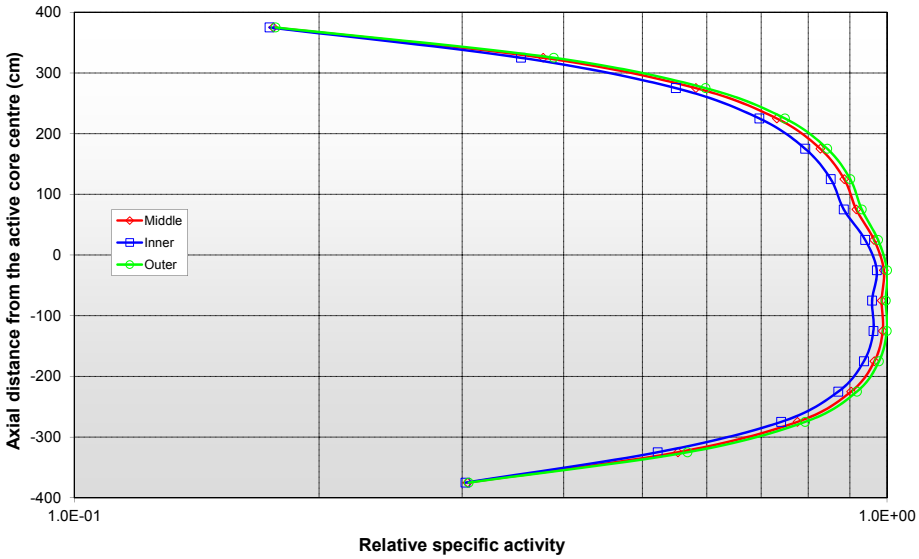

FIG. 32. Spatial distribution of Cl-36 specific activities in the different segments (see FIG. 3 b)) of the graphite blocks at RFS.

The maximal difference of the modelling results for H-3 specific activity (FIG. 30) is nearly 4 %, while the minimal is less than 0.01 %. For C-14 (FIG. 31) and Cl-36 (FIG. 32) specific activities these differences are higher – maximal differences are 12 % and 10 %, respectively, whereas minimal differences are ~1 %. Although the differences of the activities of these radionuclides are not high, but results for C-14 (FIG. 31) and Cl-36 (FIG. 32) gives clear indication that their specific activities are directly related to the thermal neutron fluxes distributions in the graphite blocks. Specific activities of C-14 and Cl-36 are higher in the outer segment of the graphite block and their axial distributions profiles also correspond to the distribution profiles of the thermal neutron fluxes (FIG. 10 a)).

However, situation for H-3 (FIG. 30) specific activity is completely different speaking about its axial and radial distribution profiles, as well as correspondence to the thermal or other energy group neutron flux. Its activity is equally distributed and does not correspond to the any of neutron flux (FIG. 10). Such phenomena is determined due to the complex H-3 balance during irradiation. In this case H-3 is mostly produced from Li impurity activation and this process is caused by both – fast and thermal neutrons. The lithium has high neutron capture cross-section and burns rapidly in the places where neutron fluxes are most intensive. Thus due to the short half-life of tritium its activity starts to decrease during prolonged irradiation in the places, where intensive neutron fluxes are because lithium impurity is burned out. In opposite, in the places where neutron fluxes are not so high, not all Li impurity is burned out and thus H-3 activity is also not decreased.

3.2.4.2. Graphite rings/sleeves

The results of the induced activities for the different segments of the graphite rings/sleeves are presented in FIG. 33 for – H-3, FIG. 34 – C-14, FIG. 35 – Cl-36.

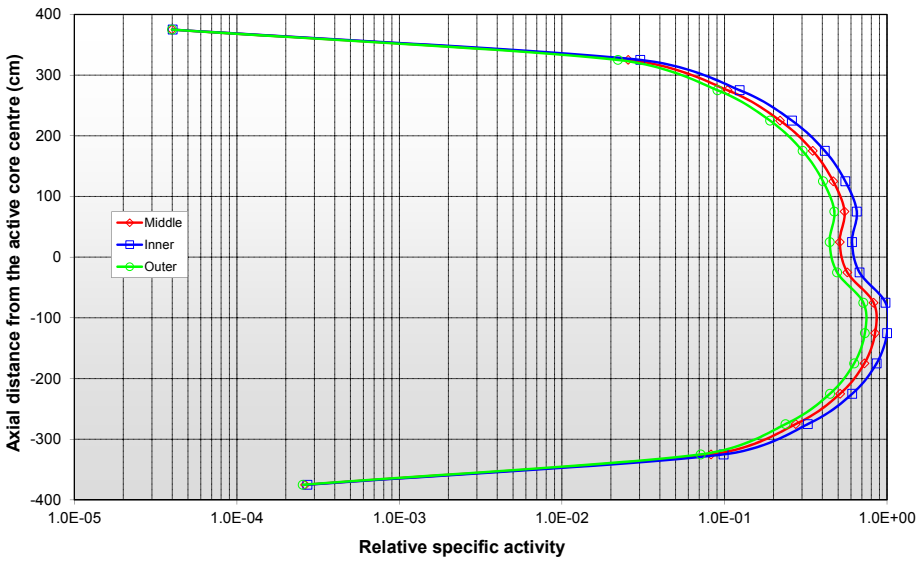

FIG. 33. Spatial distribution of H-3 specific activities in the different segments (see FIG. 3 b)) of the graphite rings/sleeves at RFS.

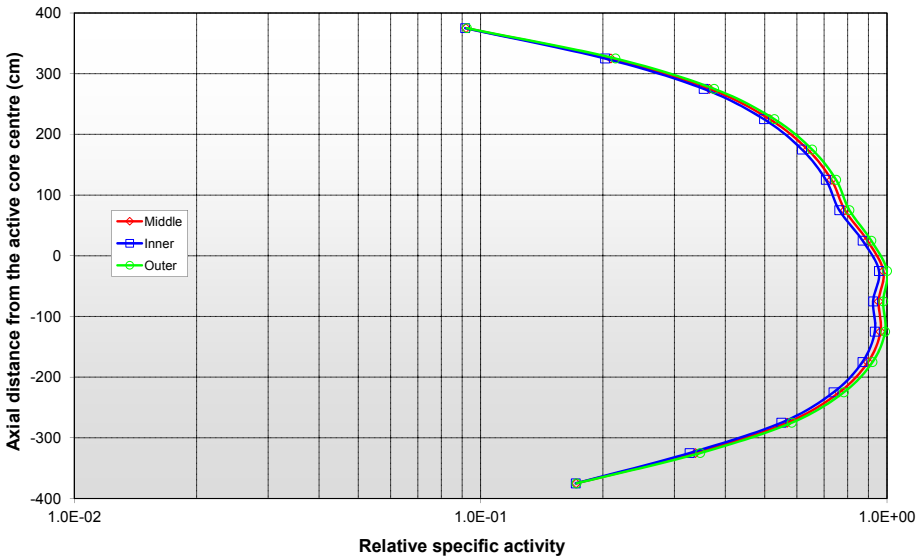

FIG. 34. Spatial distribution of C-14 specific activities in the different segments (see FIG. 3 b)) of the graphite rings/sleeves at RFS.

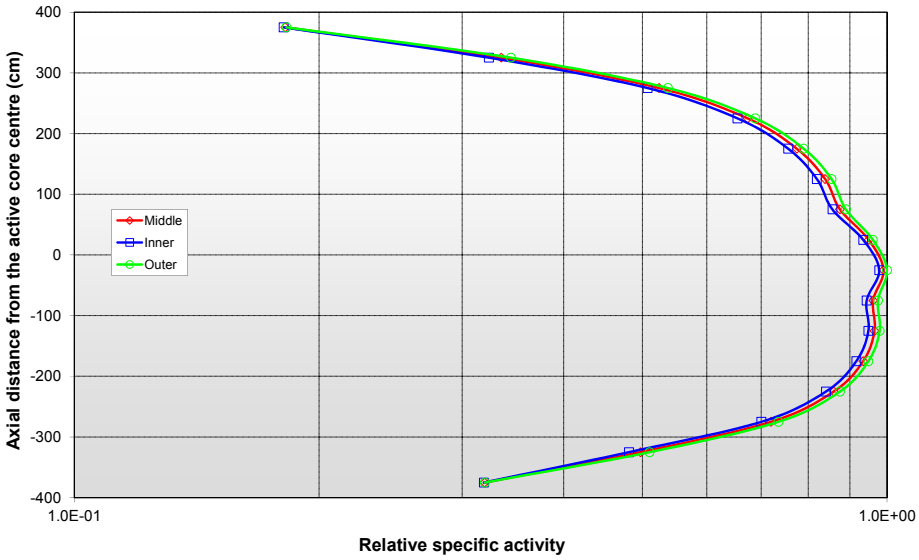

FIG. 35. Spatial distribution of Cl-36 specific activities in the different segments (see FIG. 3 b)) of the graphite rings/sleeves at RFS.

The variation characters of specific activities for each of the selected radionuclides is the same in all three segments. The average differences along the height of graphite rings/sleeves segments are ~5 % for C-14 (FIG. 34), ~4 % for Cl-36 (FIG. 35) and higher for H-3 – ~33 % (FIG. 33).

The maximal difference of modelling results for H-3 specific activity (FIG. 33) is nearly 38 %, while minimal is less than 1 %. For C-14 (FIG. 34) and Cl-36 (FIG. 35) specific activities these differences are lower – maximal differences are ~6 % whereas minimal differences are below 1 %.

Similar to the graphite blocks, the differences of specific activities of the selected radionuclides are not big, but results for C-14 (FIG. 34) and Cl-36 (FIG. 35) gives clear indication that their activities are directly related to the thermal neutron fluxes in the graphite rings/sleeves. Specific activities of C-14 and Cl-36 are higher in the outer segment of the rings/sleeves and their axial distributions profiles correspond to the distribution profiles of thermal neutron fluxes (FIG. 11 a)).

However, distribution profile for H-3 specific activity is different. Results of H-3 (FIG. 33) gives clear indication that its activities are directly related to the fast neutron fluxes distributions in the segments of graphite rings/sleeves. The specific activity of H-3 is higher in the inner segment of the graphite rings/sleeves and its axial distributions profiles also correspond to the distribution profiles of the fast neutron fluxes (FIG. 11 c)). Furthermore, H-3 distribution is completely different compared to its distribution in the graphite blocks segments (FIG. 30). This is basically determined by the fact, that for the graphite rings/sleeves there is no Li impurity and consequently there is no H-3 production from lithium activation. H-3 here is produced from carbon and other impurities interactions with fast neutron flux mainly.

4. CONCLUSIONS

The performed evaluation of the neutron fluxes distribution and induced activities modelling in the graphite components of RBMK-1500 reactor, allows to summarise that within the frame of the analysed data and assumptions made in this work:

— Neither analysed fuel type or its burnup nor the analysed data libraries have a critical influence on the modelled neutron flux intensities, energetic and spatial distributions:

- Average differences for thermal, resonance, fast and total neutron fluxes obtained using three different data libraries are respectively up to 3 %, 4 %, 4 % and 3 % for graphite rings/sleeves and blocks (except fast neutron flux for graphite blocks – up to 8 %);
- Average differences for thermal, resonance, fast and total neutron fluxes obtained using three different nuclear fuel compositions are respectively up to 8 %, 15 %, 18 % and 7 % for graphite rings/sleeves and blocks (except thermal neutron flux for graphite rings/sleeves – up to 10 %);

— For the maximal impurities concentrations modelling case, the specific activity of the graphite blocks of both Units is of 10^8 Bq/g at RFS and this is higher than that of the graphite rings/sleeves (less than 10^7 Bq/g at RFS) during analysed cooling time;

— Comparing the modelled total specific activities of Unit 1 and Unit 2 graphite components, the later have up to several percent higher specific activities, due to the longer operation time producing higher thermal power;

— For the minimal impurities concentrations modelling case, specific activity of graphite blocks is two orders of magnitude lower, while specific activity of graphite rings/sleeves is several times lower compared to the maximal impurities concentrations cases. This indicates the importance of proper knowledge of the materials compositions;

— There is no significant differences of resonance and total neutron fluxes in the inner, middle and outer graphite blocks' segments (up to 3 %), but thermal neutron fluxes are up to 10 % higher in the outer segments while the fast fluxes are up to 30 % higher in the inner. For the graphite rings/sleeves situation is similar but the differences are about 2 times lower;

— The differences of the induced activities in the analysed segments of the graphite components are directly related to the differences of the neutron fluxes in them. Thus, these differences are determined by differences of dominant neutron fluxes for the particular radionuclide production.

REFERENCES

[1] INTERNATIONAL ATOMIC ENERGY AGENCY, Radiological Characterization of Shut Down Nuclear Reactors for Decommissioning Purposes, IAEA-TRS-389, Vienna, IAEA (1998).

[2] ALMENAS, K., KALIATKA, A., UŠPURAS, E. Ignalina RBMK-1500: A source book. 2nd ed. Kaunas, Lithuanian Energy Institute, 1998. 196 p.

[3] IGNALINA NPP SAFETY ANALYSIS REPORT, Ignalina, 1996.

[4] SAFETY ANALYSIS REPORT FOR INPP UNIT 2, Ignalina, 2003.